PB-215 548

THE EFFECT OF SMALL SURFACE WAVES ON INTERFACIAL MASS TRANSFER

Kurt Muenz

Maryland University
College Park, Maryland

1965

DISTRIBUTED BY:

NTIS

National Technical Information Service
U. S. DEPARTMENT OF COMMERCE
5285 Port Royal Road, Springfield Va. 22151

WP-00323

PB 215 548

Research Report

on

THE EFFECT OF SMALL SURFACE WAVES

ON

INTERFACIAL MASS TRANSFER

Reproduced by
NATIONAL TECHNICAL
INFORMATION SERVICE
U S Department of Commerce
Springfield VA 22151

Department of Chemical Engineering
University of Maryland
College Park, Maryland

APPROVAL SHEET

Title of Dissertation: THE EFFECT OF SMALL SURFACE WAVES ON INTERFACIAL MASS TRANSFER

Name of Candidate: Kurt Muenz
Doctor of Philosophy, 1965

Dissertation and Abstract Approved: _____
Joseph M. Marchello
Associate Professor
Chemical Engineering

Date Approved:

Details of illustrations in this document may be better studied on microfiche.

VITA

Name: Kurt Muenz.

Permanent address: 9400 Adelphi Road, Adelphi, Maryland.

Degree and date to be conferred: Ph.D., 1965.

Date of birth: April 17, 1937.

Place of birth: Glauberg, Germany.

Secondary Education: Bronx High School of Science, 1953.

Collegiate institutions attended	Degree	Date of Degree
City College of New York	B.S.	1958
Yale University	M.E.	1959
University of Maryland	Ph.D.	1965

Major: Chemical Engineering.

Minor: Mathematics.

Publications: Technique for Measuring Amplitudes of Small Surface Waves, K. Muenz and J. M. Marchello, Review of Scientific Instruments, 35, 953 (1964).

Positions held: Research Chemical Engineer, Allied Chemical Corporation, Morristown, New Jersey.

Research Chemical Engineer, FMC Corporation, Baltimore, Maryland.

ABSTRACT

Title of Dissertation: THE EFFECT OF SMALL SURFACE WAVES ON INTERFACIAL MASS TRANSFER

Kurt Muenz, Doctor of Philosophy, 1965

Dissertation directed by: Professor Joseph M. Marchello

A quantitative experimental program, to determine the effects of small surface waves on interfacial mass transfer was undertaken. In addition, pertinent mass transfer and hydrodynamic theory is presented and discussed.

The particular scheme explored is that of transfer from the gas phase into a liquid (absorption), with water as the liquid throughout all experiments. The substances absorbed were Oxygen, Helium, Carbon Dioxide and Propylene. They were present as essentially pure gases. Small amplitude, progressive two dimensional waves were mechanically generated at the liquid surface. For each system, control experiments with non-waved surfaces were also carried out. Unsteady state runs were made and total gas absorbed was measured with time.

A separate series of experiments was undertaken to relate fundamental wave properties for the hydrodynamic system. Thus relationships between mass transfer and frequency could also be judged in terms of amplitude and wave length. In the course of this work, an original optical method for measuring small wave amplitudes was devised. The amplitude measurements indicated the importance of viscous effects,

Ic

which limit the scope of pertinent hydrodynamic theory.

A mathematical model based on governing diffusion equations and theoretical hydrodynamic relationships, is attempted. Its value is limited by calculation difficulties. A second model, based on an empirical effective diffusivity in the equations governing molecular diffusion is presented. This model is used to analyze experimental data and effective diffusivity is obtained as a function of wave frequency. In both wave and no wave cases, this effective diffusivity is always significantly larger than the molecular diffusivity.

Based on these results, marked increases in mass transfer over that predicted by molecular diffusion, is indicated for the no wave control runs. This highly significant observation is explained by the presence of natural convection motions, due to density and surface tension variations. The inception of waves appears to damp out these natural motions. Variation of mass transfer rate with frequency is correlated in terms of pertinent dimensionless quantities. The principal mechanism for increased mass transfer due to waves is judged to be the increase in fluid activity due to secondary drift motions of liquid particles.

THE EFFECT OF SMALL SURFACE WAVES

ON

INTERFACIAL MASS TRANSFER

by
Kurt Muenz

Dissertation submitted to the Faculty of the Graduate School of the University of Maryland in partial fulfillment of the requirements for the degree of Doctor of Philosophy
1965

Ie

ACKNOWLEDGEMENT

The author wishes to express his appreciation to the Division of Water Supply and Polution Control of the United States Department of Health Education and Welfare for the support of this research under Public Health Service Grant #WP 00323.

Many thanks are also extended to the entire staff of the Department of Chemical Engineering of the University under Professor R. B. Beckmann. In particular the guidance of Professor J. M. Marchello was invaluable. His enthusiasm and drive for the science of Chemical Engineering continue to be a source of inspiration.

Finally, the author wishes to express his indebtedness to his wife Eleanor, for her interest and encouragement and her work as a mathematics teacher during the period of this research.

TABLE OF CONTENTS

Chapter		Page
ACKNOWLEDGEMENT		ii
INTRODUCTION		1
I.	LITERATURE SURVEY	3
II.	ABSORPTION THEORY	10
III.	MEASUREMENT OF WAVE PROPERTIES	30
IV.	MASS TRANSFER EXPERIMENTS	52
V.	ANALYSIS AND DISCUSSION	66
VI.	CONCLUSIONS	105
APPENDIX A. -	LISTING OF DATA AND TABULATED QUANTITIES	108
APPENDIX B. -	EXPERIMENTAL ERROR ESTIMATION FOR MASS TRANSFER EXPERIMENTS	122
NOTATION		124
LITERATURE CITED		128

LIST OF TABLES

Table		Page
3-1.	CONSTANTS FOR EQUATION (3-15).	49
5-1.	PSUEDO STEADY STATE FILM THICKNESS . . .	79
5-2.	GRASHOF NUMBER	86
5-3.	SURFACE TENSION NUMBER	93
5-4.	VALUES OF ψ_s, EQUATION (5-37).	96
5-5.	VALUES OF K_1, EQUATION (5-39).	98
5-6.	VALUES OF ψ, EQUATION (5-41).	101
A-1.	AMPLITUDE DATA	109
A-2.	SOLUBILITY AND DIFFUSIVITY DATA.	111
A-3.	OPERATING SPECIFICATIONS	113
A-4.	MASS TRANSFER DATA, OXYGEN - WATER . . .	114
A-5.	MASS TRANSFER DATA, PROPYLENE - WATER. .	116
A-6.	MASS TRANSFER DATA, HELIUM - WATER . . .	117
A-7.	MASS TRANSFER DATA, CARBON DIOXIDE - WATER	119
A-8.	EFFECTIVE DIFFUSIVITY AND DIMENSIONLESS GROUPS.	121

LIST OF FIGURES

Figure		Page
1.	Schematic Wave Diagram.	34
2.	Light Intensity Pattern	35
3.	Wavelength Measurement, 500 CPM . . .	36
4.	Ripple Tank	41
5.	Amplitude Measuring Equipment	43
6.	Typical Light Pattern and Photographs	44
7.	Wavelength vs. Frequency for Water. .	46
8.	Reciprocal Amplitude vs. Distance from Generating Surface.	47
9.	Amplitude vs. Frequency	50
10.	Water Deaeration Equipment.	56
11.	Mass Transfer Equipment	59
12.	Oxygen Absorption With Waves.	69
13.	Propylene Absorption With Waves . . .	70
14.	Helium Absorption	71
15.	Carbon Dioxide Absorption With Waves.	72
16.	Carbon Dioxide Absorption With No Waves	73
17.	Oxygen Absorption With No Waves . . .	74
18.	Propylene Absorption With No Waves. .	75
19.	Experimental Propylene Absorption Data	77

LIST OF FIGURES (Continued)

Figure		Page
20.	Effective Diffusivity for No Wave and Driven Runs.	81
21.	Role of Bouyant Forces in No Wave Case.	87
22.	Influence of Frequency on Effective Diffusivity.	99
23.	Effect of Molecular Diffusivity . . .	103

INTRODUCTION

Mass transfer is an important component of many processes, especially in the chemical and petroleum industries. In the fields of sanitation and water treatment, gas absorption into reservoirs and tanks is often the controlling step in aeration, oxidation and evaporation processes. Waves or ripples frequently occur on the surface of such facilities and their effect on mass transfer is of interest. In addition, workers in mass transfer research have observed that surface waves are a naturally occurring phenomena in multiphase experiments. For these reasons, quantitative studies of the effect of surface waves on mass transfer are in order. Such a study has been the objective of this dissertation.

Since there are many types of surface waves and multiphase mass transfer systems, it was decided to confine this investigation to progressive two dimensional small amplitude waves with pure gas absorption into water. This was based on the need for information in this area, the relative experimental simplicity and the availability of physical property data.

In the course of working toward a goal such as that outlined above, an unexpected experimental result affecting a broader more fundamental area is often encountered. In the

case of this dissertation, such an observation occurred with regard to the unusual behavior of no wave control runs. This phenomena has been given considerable treatment in the discussion section, since it has significance well beyond the experimental limits of the present work.

In the chapters that follow, background and literature is first reviewed. Then pertinent hydrodynamic and mass transfer theory is presented. This is followed by chapters on the details and results of hydrodynamic and absorption experiments. Theory and experiment are related in the analysis and discussion section and the resulting conclusions summarized in the final chapter. Tables and figures directly pertinent to details of the written material are presented with the text, while more general data and property listings are in the Appendix.

CHAPTER I

LITERATURE SURVEY

A quantitative mass transfer study should be based on a knowledge of existing flow conditions and diffusion mechanisms. For the particular case of transfer across a waved interface, a search of the literature showed a considerable quantity of prior work on the flow phenomena involved, but little concerning diffusion. It is convenient to group together pertinent references on the occurrence and effect of interfacial phenomena on mass transfer and other engineering studies, and present hydrodynamic references separately.

The preceding paragraph suggests the first two subdivisions of this chapter. The third deals with wave generating and measuring equipment, while the final section is concerned with correlations and listings of diffusivity, solubility and surface tension data. In general, but with some exceptions, the literature cited deals specifically with gas-liquid systems.

A. Fluid Interface Phenomena in Engineering Studies

Investigations of liquid films in gravity flow down the surface of a vertical wetted wall column have been carried out by a number of workers (18, 23, 27, 55, 66). Other

techniques employed liquid films running over a sphere (18) and liquid jets (45, 50). King, Boyle and Ogle (28) have given a theoretical explanation for the oscillations observed in water flowing down a slotted trough, which is similar to earlier investigations of oscillating jets (1).

Interfacial effects in absorption have been studied by Bond and Donald (8) using the absorption of ammonia from a gas stream in a wetted wall column. A minimum flow rate was determined, below which the film breaks down and there is a considerable reduction in liquid area. The results are interpreted as being due to a difference in surface tension between the point where the film breaks and the main bulk of the liquid. This explanation is based on the Marangoni Effect, wherein movement on an interface is caused by longitudinal variations of the interfacial tension. Chiang and Toor (13) discuss interfacial resistances for short contact times with the Oxygen-Water system.

Hanratty and co-workers (24, 25, 33, 34) have worked on the wave phenomena occurring with concurrent air and water flow. Conditions for initiation of roll waves (in very shallow water streams) were investigated (25). Inception of waves and eddy formation on a liquid film flowing down a smooth plate is dealt with by Tailby and Portalski (57). Levich (31) considers mass transfer in conjunction with a vertical liquid film with a waved surface.

The majority of these investigators, regardless of experimental method, have noted that ripples and waves on the

surface, even at low Reynolds Number, cause abnormally high mass transfer rates. Striba and Hurt (55) have pointed out that the increase in area due to ripples is not enough to cause the increased mass transfer. They proposed some degree of turbulence as an explanation for this phenomenon. In general, the literature does not present any method for differentiating between area and hydrodynamic contributions to the rate of mass transfer.

Furthermore, the nature of the waves and ripples observed has not necessarily been identical. Scriven and Pigford (50) observed standing waves on a stagnant surface near the liquid exit in wetted wall, rotating drum and jet absorber devices. Grimley (23) and Jackson (27) have observed roll waves in wetted wall columns. The different types of waves should have different effects on mass transfer.

Scriven (49) has developed the equations for the dynamic behavior of a liquid interface. In an earlier analysis Sternling and Scriven (52) used a simplified mathematical model to analyze the mechanism supplying energy to interfacial turbulence. They posed the problem as being hydrodynamic with diffusion and surface movement acting as coupled processes. The methods of conventional linear stability were used to determine conditions for the onset of instability and the nature of the dominant disturbance. Their resulting equations relate interfacial tension and concentration profile near the surface to the interfacial turbulence level. It should be noted that this reference deals with an initially

flat surface.

The subject of natural convection caused by density differences is of interest in undisturbed situations. Bird, Stewart and Lightfoot (6) point out the analogy to thermal natural convection. Lemlich and Levy (30) studied the effect of a vibrating surface on natural convective mass transfer for the case of a solid-gas interface. Levich (32) presents an analysis of natural convection due to density gradients opposing the gravitational field for the case of diffusion and chemical reaction occurring simultaneously.

Chapman (12) has investigated the absorption of Carbon Dioxide into water on the surface of which a periodic wave motion was propagated. The experimental relationships between wave length and frequency was found to check that predicted by classical wave hydrodynamics. The apparatus used developed frequencies up to 550 cycles per minute. Absorption measurements for non-disturbed and waved surfaces were made and values of eddy diffusivity calculated. Because of difficulty in determining wave amplitude, it was difficult to correlate these values with wave properties.

B. Wave Hydrodynamics

The hydrodynamics associated with surface waves have been studied since the nineteenth century by, among others, famous physicists and mathematicians such as Poisson, Airy, Stokes, Kelvin, Rayleigh and Boussinesq.

Through the years a "classical theory" has evolved for

flat surface.

The subject of natural convection caused by density differences is of interest in undisturbed situations. Bird, Stewart and Lightfoot (6) point out the analogy to thermal natural convection. Lemlich and Levy (30) studied the effect of a vibrating surface on natural convective mass transfer for the case of a solid-gas interface. Levich (32) presents an analysis of natural convection due to density gradients opposing the gravitational field for the case of diffusion and chemical reaction occurring simultaneously.

Chapman (12) has investigated the absorption of Carbon Dioxide into water on the surface of which a periodic wave motion was propagated. The experimental relationships between wave length and frequency was found to check that predicted by classical wave hydrodynamics. The apparatus used developed frequencies up to 550 cycles per minute. Absorption measurements for non-disturbed and waved surfaces were made and values of eddy diffusivity calculated. Because of difficulty in determining wave amplitude, it was difficult to correlate these values with wave properties.

B. Wave Hydrodynamics

The hydrodynamics associated with surface waves have been studied since the nineteenth century by, among others, famous physicists and mathematicians such as Poisson, Airy, Stokes, Kelvin, Rayleigh and Boussinesq.

Through the years a "classical theory" has evolved for

waves of small amplitude and wave length (compared to liquid depth). This theory is presented in many articles and texts, among them Stoker (53), who does not consider surface tension effects and Clark (15), Coulson (16) and Page (41) who do. The theory is based on assuming a non-viscous, compressible liquid and using expansion of properties in terms of a parameter to obtain a first order solution. This mathematical procedure is presented by Wehausen and Laitone (62). These authors give a very extensive presentation and bibliography on the general topic of wave hydrodynamics (61). The classical first order theory is applicable to both progressive and standing waves and relates velocity potential to position and time. It yields an equation for wave profile and shows the relations between amplitude, wave length and frequency for two dimensional wave motion.

Experimental verification of various facets of first order theory (for water) were made by Ursell et al. (59), Yu and Ursell (68) and Ruellan and Wallet (46). This last reference contains an excellent photographic verification of the particle paths predicted by theory.

A considerable amount of literature deals with more complex cases, wherein one or more of the simplifying assumptions of the classical theory are not made. Crapper (17) and Tadjebakhsh and Keller (56) deal with terms beyond the first order in power expansions. Longuet-Higgins (35, 36) and Whitham (64) consider second order particle drifts (compared with closed particle paths of the classical theory), wherein

the effect of viscosity is not neglected. Wehausen and Laitone (63) summarize the mathematical treatment for standing waves that damp with respect to time, while Carry (10) considers progressive waves damping with distance. All of these considerations greatly increase the mathematical complexity of the theory.

C. Wave Generating and Measuring Equipment

The most applicable device for generating small waves, is the ripple tank (14, 15, 48). This is frequently used to demonstrate wave phenomena to beginning physics students. Such a device generally contains an electrically operated wave generator capable of producing small, relatively high frequency waves in a finite depth tank and has a stroboscopic mechanism for determining wave length and frequency of the waves. Other wave generating devices are a piston wave maker (59) and an oscillating circular cylinder (68).

The most common method for measuring wave profiles and amplitudes is by use of variable capacitance level sensors (3, 58, 65, 67). With these the variation of liquid height at a point is measured by the change of capacitance of an immersed coated wire. The accuracy of this device is limited by a false height indication due to the meniscus resulting from surface tension between the liquid and coating. Use of micrometer gages (4) and resistance probes (4) is subject to the same error source. Various optical methods are presented (20, 38, 44). The photographic method of Muenz and Marchello

was devised in conjunction with the work covered by this dissertation. It is described in Chapter III and in a separately published paper (39). The method is in part based on previous treatments of the light refraction properties of waved surfaces given by Shenck (51) and Schooley (48).

D. Physical Properties

There are a number of correlations of surface tension and temperature, among them those of Othmer and Gilmont (40) and Brock and Bird (9), based on critical properties. Very little has been written about the effect of solute concentration on surface tension. Ferguson (21) noted that changes of the order of 1/2 of 1% had been observed when water was saturated with air. Kuper and Trevena (29) devised a rough method for calculating the effect of small concentrations of gases, making use of van der Waal's constants.

Vivian and King (60) present dilute molecular diffusivity data for different systems including those dealt with in this dissertation. The data include measurements by the authors as well as results of previous investigators.

The International Critical Tables (26) serve as the major source of equilibrium solubility data. This is supplemented by the Propylene solubility data of Azarnoosh (2).

CHAPTER II

ABSORPTION THEORY

A. Formulation and Discussion of a Mathematical Model

A theoretical analysis of gas absorption to a liquid contained in a finite rectangular tank and undergoing wave motion is desired.

As a first approach, a mathematical model in the form of a differential equation, relating concentration of the absorbing gas in the liquid to position and time, is attempted. This model is based on the assumption that all particle motions (bulk flow) in the liquid are due to surface waves.

1. Diffusion Equation. The basis for the model is the well known mass transfer analogy to the Fourier-Poisson Heat Transfer Equation (5). This is here derived. Consider a control volume of liquid V with a surface S. Let C be the molar concentration of dilute component (absorbing gas) and let θ be time. Then the rate of accumulation of the dilute component (in moles/hour) is given by

$$\int_V (\partial C/\partial \theta)\, dV \quad . \tag{2-1}$$

The net flux (output—input) is then

$$\int_S \bar{J} \cdot d\bar{A} \tag{2-2}$$

where $\bar{J}$ is the total flux vector at a point on the surface

and $d\bar{A}$ is equal to $\bar{n}.dS$. $\bar{n}$ is the outward unit normal vector. Making the usual statement of conservation of mass, output—input equals accumulation

$$- \int_S \bar{J}\cdot d\bar{A} = \int_V (\partial C/\partial \theta)\, dV \quad . \tag{2-3}$$

Since only very dilute solutions are dealt with, the assumption of no coupling of fluxes is made; i.e., there is no bulk velocity due to the diffusion of the dilute component. Then

$$\bar{J} = \bar{J}_F + \bar{J}_d = \bar{v}\cdot C - D\nabla C \quad . \tag{2-4}$$

The right hand terms represent transfer by bulk flow and by diffusion (Fick's Law). $\bar{J}_f$ is the total surface flux (of dilute component) due to bulk flow, $\bar{J}_d$ the total surface flux due to molecular diffusion, $\bar{v}$ the bulk velocity and D the molecular diffusivity of the solute. Thus

$$- \int_S (\bar{v}\cdot C - D\nabla C)\cdot d\bar{A} = - \int_V (\partial C/\partial \theta)\, dV \quad . \tag{2-5}$$

Applying the divergence theorem to the left side of (2-5) get

$$- \int_V \nabla\cdot(\bar{v}\cdot C - D\nabla C)\cdot dV = - \int_V (\partial C/\partial \theta)\, dV \tag{2-6}$$

and since V can be chosen arbitrarily small this becomes

$$\partial C/\partial \theta + \nabla\cdot(\bar{v}C) - \nabla\cdot(D\nabla C) = 0 \quad . \tag{2-7}$$

For dilute solutions D is assumed to be constant and for an incompressible fluid

$$\nabla \cdot \bar{v} = 0 \quad . \tag{2-8}$$

Then

$$\partial C/\partial \theta + \bar{v} \nabla C = D \nabla^2 C \tag{2-9}$$

and in two dimensions

$$\partial C/\partial \theta + u(\partial C/\partial x) + v(\partial C/\partial y) = D(\partial^2 C/\partial x^2 + \partial^2 C/\partial y^2) \tag{2-10}$$

where u and v are respectively the x and y direction components of $\bar{v}$. Thus, if expressions for u and v in terms of the independent variables x, y and θ can be obtained, (2-10) is the general equation describing mass transfer.

2. Wave Hydrodynamics. The velocity coefficients for equation (2-10) may, in principle, be obtained from wave hydrodynamics. Appeal is made to the wealth of literature on this subject. Since the details are quite lengthy, even for specific types of wave motion, little derivation is presented here. Rather, reference is made to the extensive presentation and review of the subject by Wehausen and Laitone (61) and by Coulson (16).

Due to the nature of experiments performed in conjunction with this dissertation, only "progressive, two dimensional waves" in a rectangular tank of finite depth are considered. In dealing with such waves, the usual assumptions are the existence of a tank of infinite length and a steady fluid motion, periodic with respect to time and direction of wave generation.

Since rigorous mathematical solutions to liquid wave problems are virtually impossible, a technique of expansion in powers of a parameter is used to approximate velocity, pressure and vertical surface displacement. In general, only terms up to the first order are retained in deriving hydrodynamic relationships, yielding a "first order theory". The details of this procedure are given by Wehausen and Laitone (62).

Other general assumptions and conditions are lack of tank sidewall effects, limitation to incompressible fluids and amplitude of waves being small in comparison to depth of liquid.

Two situations are of interest. The first concerns the case where effects of viscosity may be neglected. In such wave motion no attenuation (i.e., amplitude damping in the direction of wave generation) is expected, since no mechanism for energy dissipation is available. This case is experimentally approachable with liquids of low viscosity and relatively low fluid particle velocities. The second case excludes the inviscid assumption and amplitude attenuation is expected.

For the inviscid case, since the liquid is assumed incompressible ϕ may be introduced such that

$$u = \partial\phi/\partial x, \quad v = \partial\phi/\partial y \quad . \tag{2-11}$$

The x-axis is taken at the (undisturbed) free surface with y being positive in the upward vertical direction. x is taken

as positive in the direction of wave generation. Summarizing the result of wave hydrodynamics for this "deep water" case, a solution of the form

$$\phi = (B_1 e^{my} + B_2 e^{-my})\cos(mx-\omega\theta) \qquad (2\text{-}12)$$

is sought, where $m = \lambda/2\pi$, λ = wave length, $\omega = 2\pi f$ and f is the wave frequency. B_1 and B_2 are constants. The equation of continuity states that

$$\partial^2\phi/\partial x^2 + \partial^2\phi/\partial y^2 = 0 \quad . \qquad (2\text{-}13)$$

From "first order" theory considerations the following boundary conditions hold.

$$\partial\eta/\partial\theta = v \quad \text{at } y = 0 \qquad (2\text{-}14)$$

$$-\partial\phi/\partial y = (1/y)(\partial^2\phi/\partial\theta^2) - (\sigma/\rho g)(\partial^2(\partial\phi/\partial y)/\partial x^2) \quad \text{at } y = 0 \qquad (2\text{-}15)$$

$$\partial\phi/\partial y = 0 \quad \text{at } y = -h \text{ (fixed surface)} \qquad (2\text{-}16)$$

where h is the depth of liquid, σ the interface surface tension, ρ the liquid density, η the vertical displacement at the free surface and g the acceleration due to gravity. Inserting the boundary conditions into (2-12) the following relations are obtained. (See Coulson (16) and Clark (15).)

$$\phi = -A\cosh(m(y+h))\cos(mx - \omega\theta) \qquad (2\text{-}17)$$

where A is a constant.

$$c^2 = \omega^2/m^2 = (g/m + m\sigma/\rho)\tanh(mh) \qquad (2\text{-}18)$$

$$\eta = (A/c)\sinh(mh)\sin(mx - \omega\theta) \quad . \qquad (2\text{-}19)$$

The wave surface is sinusoidal and of the form

$$\eta = a \sin(mx - \omega\theta) \tag{2-20}$$

where a is the wave amplitude. Therefore,

$$A = -ac/\sinh(mh) \quad . \tag{2-21}$$

From (2-19)

$$u = \partial\phi/\partial x = Am \cosh(m(y+h))\sin(mx - \omega\theta) \tag{2-22}$$

$$v = \partial\phi/\partial y = -Am \sinh(m(y+h))\cos(mx - \omega\theta) \quad . \tag{2-23}$$

Expressions (2-22) and (2-23) are the velocity coefficients for (2-10) for the inviscid case.

For the case where viscosity is not neglected the equations are the equation of continuity

$$\partial u/\partial x + \partial v/\partial y = 0 \quad , \tag{2-24}$$

a form of the Navier-Stokes equation

$$\partial \bar{v}/\partial \theta = -1/\rho \operatorname{grad}(p + \rho gy) + \nu\nabla^2 v \quad , \tag{2-25}$$

where ν is the kinematic viscosity and

$$\partial u/\partial y + \partial v/\partial x = 0 \tag{2-26}$$

on the free surface. The last expression is due to the condition of mathematical continuity of the stress vector on passing through the interface. As in the inviscid case, the following apply.

$$\partial\eta/\partial\theta = v \qquad \text{at } y = 0 \qquad (2\text{-}27)$$

$$v = 0 \qquad \text{at } y = -h \quad . \qquad (2\text{-}28)$$

For the steady generation of viscous progressive waves, amplitude attenuation occurs. The necessary solution of the above set of equations must, therefore, incorporate a surface wave profile periodic with respect to time and damped periodic with respect to the direction of wave generation. Only one such solution was found in the literature (10). This solution by Carry, results in an extremely lengthy expression for a stream function from which the velocities may be calculated.

If the effect of viscosity is assumed to be significant only in the wave travel direction and not in the vertical direction, a simplified approximation may be valid. This approach was suggested by the experimental fact that even though viscous attenuation was significantly observed, relation (2-18) still held. This correlation of wave length and frequency is derived from a y-direction force balance (Bernoulli Equation--see e.g., Coulson (16)) based on a velocity potential assumption. A damped form of the surface displacement is then

$$\eta = ae^{-rx}\sin(mx - \omega\theta) \qquad (2\text{-}29)$$

where r is a constant whose value is a function of viscosity. r would have to be determined experimentally for any given wave system. By boundary condition (2-27) at y = 0

$$v = -a\omega e^{-rx}\cos(mx - \omega\theta) \qquad (2\text{-}30)$$

and from (2-28) at y=-h, v=0. Thus, if the form for the y direction velocity is

$$v = F(y)e^{-rx}\cos(mx - \omega\theta) \tag{2-31}$$

then

$$F(y) = 0 \text{ at } y = -h \tag{2-32}$$

$$F(y) = -a\omega \text{ at } y = 0 \tag{2-33}$$

and F(y) is not uniquely determined. However, by the assumption of lack of viscous effect in the y direction, the dependence on depth might be approximated by the exponent form of the inviscid case; i.e.,

$$F(y) = B \sinh(m(y+h)) \tag{2-34}$$

where

$$B \sinh(mh) = -a\omega \tag{2-35}$$

and (2-33) is satisfied. Thus,

$$v = B \sinh(m(y+h))e^{-rx}\cos(mx - \omega\theta) \tag{2-36}$$

Applying (24) and making use of the fact that when x is infinite all motion is damped and hence u and v are zero, an expression for u is obtained.

$$u = -Bm \cosh(m(y+h))(e^{-rx}/\ r^2+m^2)(-r\cos(mx - \omega\theta) + m \sin(mx - \omega\theta)) \tag{2-37}$$

(2-36) and (2-37) give velocity coefficient expressions for

equation (2-10).

It must be pointed out that (2-36) and (2-37) do not satisfy boundary condition (2-26). They are, therefore, only a convenient approximation.

It is noteworthy to examine the particle paths predicted by these velocity expressions. This is done by integrating the velocity expressions with respect to time, holding x and y constant. (See Coulson (16).) Let Y be the y direction displacement from the mean (at rest) position of a particle whose at rest position is (x, y). Let X be the x direction displacement from this mean position. Then

$$Y = \int_v d\theta = -(B/\omega)\ \sinh(m(y+h))\ e^{-rx}\sin(mx - \omega\theta) \qquad (2\text{-}38)$$

$$X = \int_u d\theta = -(Bm/\omega)\ \cosh(m(y+h))(e^{-rx}/r^2+m^2)(r\ \sin(mx - \omega\theta) + m\ \cos(mx - \omega\theta)\ . \qquad (2\text{-}39)$$

Upon examination of the amplitude attenuation data of the following chapter, it is seen that $r \ll m$ and hence $r^2 \ll m^2$ and can be neglected in the r^2+m^2 term. Thus,

$$X = -(rB/m\omega)\ \cosh(m(y+h))e^{-rx}\sin(mx - \omega\theta) - (B/\omega)\ \cosh(m(y+h))e^{-rx}\cos(mx - \omega\theta)\ . \qquad (2\text{-}40)$$

These expressions, when compared to the eliptical partical paths predicted by the inviscid theory (see Coulson (16)) indicate the particle paths to be slightly distorted forms of the elipse with the vertical axis slightly tilted. Since r/m is small for the experimental situation in question and the sine function is bounded absolutely by 1, the distortion term

may be neglected. Thus,

$$Y = -e^{-rx}(B/\omega)\sinh(m(y+h))\sin(mx - \omega\theta) \quad (2\text{-}41)$$

$$X = -e^{-rx}(B/\omega)\cosh(m(y+h))\cos(mx - \omega\theta) \quad (2\text{-}42)$$

which are the expressions predicted by inviscid theory multiplied by an e^{-rx} coefficient; i.e., the elipse sizes damp out exponentially in the x direction.

The actual amplitude data for the wave apparatus used in connection with this dissertation, show that the exponential wave decay expression is inaccurate. Rather an expression of the form

$$a = 1/(\epsilon x + \beta) \quad (2\text{-}43)$$

appears more accurate. (See Chapter III)

An attempt to use this form in place of the exponential one in the previous derivation results in considerable mathematical difficulty. If the conclusions of particle path considerations connected with exponential decay are accepted, however, analogous expressions for the particle path displacements are

$$Y=(1/\epsilon x+\beta)(\sinh(m(y+h))/\sinh(mh))\sin(mx - \omega\theta) \quad (2\text{-}44)$$

$$X=(1/\epsilon x+\beta)(\cosh(m(y+h))/\sinh(mh))\cos(mx - \omega\theta) \quad (2\text{-}45)$$

Differentiating with respect to time, the velocity terms are

$$v=(-\omega/\epsilon x+\beta)(\sinh(m(y+h))/\sinh(mh))\cos(mx - \omega\theta) \quad (2\text{-}46)$$

$$u=(\omega/\epsilon x+\beta)(\cosh(m(y+h))/\sinh(mh))\sin(mx - \omega\theta) \quad (2\text{-}47)$$

and these expressions may be used in (2-10).

It must be pointed out that the substitution of such velocity expressions into (2-10) itself involves an approximation. This is due to the velocities being dependent on the mean (at rest) position of particles (a Lagrangian type of coordinate system) while equation (2-10) calls for the velocity at a fixed point in space (an Eulerian system). Since the amplitude to wave length ratios are small, the particle displacements are small. Thus the magnitude and direction of velocity of a particle at any time approximates that of the fluid at its mean position.

3. Integration of Mass Transfer Equation. Because of the complexity of the velocity terms of (2-10), no analytical integration of this equation appears possible. Rather a numerical finite difference method is called for. The known boundary conditions are

$$C(x, y, 0) = 0 \qquad (2\text{-}48)$$

$$C(x, 0, \Theta) = C_i \qquad (2\text{-}49)$$

where C_i is the equilibrium (saturated) concentration of gas being absorbed, and

$$C(x, -h, \Theta) = 0 \quad ; \qquad (2\text{-}50)$$

i.e., it is assumed that the absorbing gas does not penetrate to the tank bottom in the course of a run.

Since the boundary conditions include an initial time condition and equation (2-10) contains a first partial with

respect to time, the finite difference solution requires no iteration. Rather the concentration at a mesh point and at a given time can be expressed as a function of the previous time concentration at that mesh point and its four nearest neighbors. This value is then used in the computation of the concentrations for the next time period.

The solution is severely hampered, however, by the selection of the mesh spacing. Due to the periodic nature of the velocity coefficients, the time mesh must be a small fraction of the reciprocal of frequency, and the y direction mesh a small fraction of the amplitude. Otherwise, the true effect of the cyclic motion within the liquid would not be represented by the finite difference solution. Furthermore, the x direction spacing should be a reasonable fraction of the wave length for the same reason.

In the experimental case dealt with subsequently, these conditions require in the order of 10^5 to 1.5×10^5 space mesh points for each time period. This is estimated by taking the x direction spacing to be $\lambda/20$ and the y direction spacing to be 0.1 milimeters. Taking a time mesh to be 1/20 of the reciprocal frequency, the average run would require 5×10^5 to 10^6 time periods. Thus 5×10^{10} to 1.5×10^{11} calculations are necessary per run. Each such calculation would involve at least 50 computer operations in even the simplest case. (This is probably a very low estimate, since subroutines are necessary to compute the trigonometric and hyperbolic functions.) Thus even a computer capable of executing 2×10^5

operations per second would require in the order of 500 to 1500 hours of machine time to analyze one run. This highly prohibitive figure indicates that this approach is workable only for extremely short times and small penetration depths. Because of experimental initiation errors for short times, the analysis cannot be used to evaluate the data of this dissertation.

At this point an additional hydrodynamic factor should be emphasized. If second order terms are included in the inviscid parameter expansions for the wave properties, closed particle paths are no longer predicted. (See e.g., Longuet-Higgins (35).) This predicts the existence of a net "drift" velocity, which though slow may affect mass transfer. It is believed that viscous effects increase this drift velocity (35).

This phenomenon and the aforementioned lack of rigor and computational difficulties makes the partial differential equation model quite academic for this physical situation. This analysis has been presented, however, since it may be applicable where short time behavior is of interest. A possible example is the case of a steady state flow-mass transfer situation across a waved surface. Within short times the drift effects would be minimal. The model should be most effective in slower frequency situations where viscous effects would be less critical.

4. General Remarks. Before concluding this section it is worthwhile to discuss the possibility of turbulence connected with wave motion. The assumption of no viscous effects in most of the mathematical treatment precludes turbulent motion. Smooth steady particle flows are predicted. Analysis of these paths (See e.g., Coulson (16).) along with the paths of neighboring particles indicates that relative positions remain essentially intact in spite of considerable motion. Such a mechanism should contribute very little to increasing mass transfer rate over that of the still fluid. No increase in concentration gradient occurs.

In experimental situations where viscous effects are significant, the possibility for turbulence exists. It is conceivable that as frequency (and hence fluid velocity) increases, a transition to turbulent flow may occur. Such flow probably would be periodic on a time average basis, but would have random instantaneous fluctuations. The marked effect of such turbulent phenomena on mass transfer is well known.

The concepts of secondary drift motions and turbulence suggest a more empirical method of evaluating data, which is discussed in the following section.

B. Fick's Law Model

Equation (2-10), the mass transfer analog to the Fourrier-Poisson Equation, relates concentration to position and time. In vector form it is written as

$$\partial C/\partial \theta + \nabla\cdot(\bar{v}C) = D\nabla^2 C \qquad (2\text{-}51)$$

where $\bar{v}$ is the velocity vector. As is done for cases of fluctuating velocity, the variables are divided into fluctuating and non-fluctuating components. This procedure was first used by Prandtl (47) in turbulent flow analysis. For (2-51) the velocity and concentration become

$$v = v + v' \qquad (2\text{-}52)$$

$$C = C + C' \qquad (2\text{-}53)$$

Substituting into (2-51)

$$\partial(C + C')/\partial \theta + \nabla(v + v')(C + c') = D\nabla^2(C + C') \quad . \qquad (2\text{-}54)$$

Now each term is time averaged, making use of the rules of averaging as follows.

$$\overline{f} = f,\ \overline{f'} = 0,\ \overline{ff'} = 0,\ \overline{f'g'} \neq 0 \qquad (2\text{-}55)$$

where f and g are arbitrary properties. These rules are applied to (2-54). Assuming the variables to be stepwise continuous, the averaging can be carried out inside the differentiation. The result of these operations is

$$\partial \overline{C}/\partial \theta + \nabla(\overline{vC}) + \nabla(\overline{v'C'}) = D\nabla^2\overline{C} \qquad (2\text{-}56)$$

For this particular experimental situation $\bar{v}$ is assumed equal to zero (i.e., no net motion). Thus

$$\partial \overline{C}/\partial \theta + \nabla(\overline{v'C'}) = D\nabla^2\overline{C} \quad . \qquad (2\text{-}57)$$

The usual practice is to define an eddy diffusivity ϵ, by

the relationship

$$\nabla(\overline{v'C'}) = -\epsilon \nabla^2 \overline{C} \quad . \tag{2-58}$$

Combining (2-57) and (2-58) gives the form of Fick's Second Law

$$\partial \overline{C}/\partial \theta = (\epsilon + D)\nabla^2 \overline{C} \quad . \tag{-2-59}$$

For the purposes of empirical correlation it is assumed that the quantity $\partial^2 C/\partial x^2$ is negligible compared to $\partial^2 C/\partial y^2$ in the $\nabla^2 \overline{C}$ term. Then, dropping vector terminology, in one dimension

$$\partial C/\partial \theta = D_w(\partial^2 C/\partial y^2) \tag{2-60}$$

where D_w is an empirical "effective diffusivity". If this last assumption (regarding the x direction gradient) is valid, then D_w is equivalent to $\epsilon + D$.

Three types of flow may influence the value of D_w. The first of these may be random turbulence along particle paths associated with first order wave motion. The first order motions themselves should have little influence as discussed in the previous section. A second motion is second order or drift flow due to the waves. For the case of constant amplitude, both the inviscid theory and one wherein viscosity is taken into account (35), indicate net drift currents. These are of the order of size of the tank itself. For the case of attenuated amplitude, which occurs in the physical situation of this dissertation, no such prediction is available

It is possible that that the drift paths may be considerably smaller than the tank dimension when attenuation is important. The third motion is that arising by natural convection. This may be caused by bouyant conditions arising from slight density changes due to solution or by surface tension perturbations causing surface and associated bulk fluid motions (Marangoni Effect, see e.g., (52)).

The following boundary conditions to (2-60) hold for the physical problem at hand.

$$C\,(\,y,\,0\,) = 0 \qquad (2\text{-}61)$$

$$C\,(\,0,\,\theta\,) = C_i \qquad (2\text{-}62)$$

$$\partial C\,(\,-h,\,\theta\,)\,/\,\partial y = 0 \quad . \qquad (2\text{-}63)$$

The solution to (2-60) with this set of boundary conditions is found, using a heat transfer analogy, in the text of Carslaw and Jaeger (11). The analogy to (2-63) results from a symmetry condition inherent in the heat transfer problem of the reference. The integrated solution is

$$C=C_i - (4C_i/\pi) \sum_{n=0}^{\infty} ((-1)^n/(2n+1))e^{-R}\cos((2n+1)\pi(y+h)/2h) \qquad (2\text{-}64)$$

where R is the ratio $D_w(2n+1)^2\pi^2\theta/4h^2$. By a material balance, the total amount of gas absorbed at any time is given by

$$\Delta n = A\int_{-h}^{0} C\,dy \quad . \qquad (2\text{-}65)$$

Upon substitution of (2-64) and integration get

$$\Delta n=AC_ih(1-(8/\pi^2)\sum_{n=0}^{\infty}(1/(2n+1)^2)\,e^{-R} \quad . \qquad (2\text{-}66)$$

Ah is the total liquid volume V_L. Rearranging get

$$1-\Delta n/C_i V_L = (8/\pi^2) \sum_{n=0}^{\infty} (1/(2n+1)^2) e^{-R} \quad . \qquad (2\text{-}67)$$

Consideration of the series terms indicates that for values of $D_w \pi^2 \theta/4h^2 \geq 0.1$, the second term (n=1) of the series is less than 5% of that of the first term (n=0) and that as an approximation all but the first term may be neglected.

$$1-\Delta n/C_i V_L = (8/\pi^2)\, e^{-(D_w \pi^2 \theta/4h^2)} \quad . \qquad (2\text{-}68)$$

If empirical use of D_w is justified, a plot of $\mathrm{Ln}(1-\Delta n/C_i V_L)$ vs. θ should yield a straight line with a slope $-D_w \pi^2/4h^2$. Since Δn vs. θ is the form of the experimental data of the dissertation, this plot can be made and D_w determined experimentally. Care must be taken, that only data points corresponding to times sufficiently high so that $D_w \pi^2 \theta/4h^2$ is equal to or greater than 0.1 are used. This can be done by taking an approximate slope from the last few points of a run, calculating a rough D_w and checking this ratio. A final value of D_w can then be calculated by use of the proper data points.

For the case of runs where D_w is so low that no data points meet the above criteria, the following derivation gives a means of calculating effective diffusivity. Consider equation (2-60) with boundary conditions (2-61) and (2-62), but replace (2-63) with

$$C\ (-\infty, \theta) = 0 \quad . \qquad (2\text{-}69)$$

Thus, an assumption of a tank of infinite depth is made. This is equivalent to setting h equal to infinity in (2-64) and is justified by h being relatively large in the $D_w \pi^2 \theta / 4h^2$ ratio for the cases of small D_w. For such cases the per cent of saturation and degree of penetration is very low, which also supports the infinite depth assumption. For this case the solution to (2-60) is

$$C = C_i(1 - \text{erf}(-y/(4D_w\theta)^{0.5})) \quad . \tag{2-70}$$

For small values of y, (2-70) becomes

$$C = C_i(1 - (-y)/(\pi D_w\theta)^{0.5} + (-y)^3/12D_w\theta \ -\cdots) \quad . \tag{2-71}$$

The mass transfer flux at the surface is given by

$$N = -D_w(\partial C/\partial y)_{y=0} \quad . \tag{2-72}$$

From (2-71)

$$(\partial C/\partial y)_{y=0} = C_i/(\pi D_w\theta)^{0.5} \tag{2-73}$$

and the flux is

$$N = -C_i(D_w/\pi\theta)^{0.5} \quad . \tag{2-74}$$

The negative sign indicates that transfer occurs in the downward vertical direction. Now

$$\Delta n = A \int_{\theta_i}^{\theta} |N| \, d\theta \tag{2-75}$$

where θ_i is an effective initial time. By (2-74) and (2-75)

$$\Delta n = 2AC_i((D_w\theta/\pi)^{0.5} - (D_w\theta_i/\pi)^{0.5}) \quad . \qquad (2\text{-}76)$$

(2-76) indicates that a plot of Δn vs. $\theta^{0.5}$ should give a straight line, the slope of which can be used to evaluate D_w for the applicable cases.

CHAPTER III

MEASUREMENT OF WAVE PROPERTIES

The hydrodynamic coefficients for the partial differential equation (2-10) discussed in the previous chapter, require knowledge of wave frequency, amplitude and wave length. This chapter is concerned with the experimental methods and results connected with the measurement of these properties. The results of amplitude measurements indicated the presence of viscous effects, with their pronounced effect on wave hydrodynamics (See Chapter II).

A. Methods

1. Measurement of Frequency. A Cenco stroboscope was used to measure the frequency of the wave generator camshaft (see section B, below), which corresponded to the wave frequency. The stroboscope frequency was preset to the desired value and the variable speed drive was adjusted until the motion of an "Allen Screw" on the shaft, appeared to cease. Mechanical details of the generator are discussed below.

2. Measurement of Wave Length. In each case wave length was determined by photographing the tank from above in synchronization with a flash of light aimed at the surface. The

resulting picture consists of alternating dark and light bands caused by the lens effect on the surface in reflecting light. Wave lengths were determined by measuring (with proper scaling) the distance on the picture, between similar points of successive dark bands (e.g., the center of the band). Alternatively, the procedure was modified such that a span of 5 to 6 bands was measured and divided by the number of waves (bands).

The source of light was an electronic flash unit rated at 1/1500 second, so that wave motion was essentially "frozen". Figure 3 is an example of the pictures taken (at 500 CPM). Note the scale placed at the surface level which was used for scaling.

3. Measurement of Amplitude. Amplitude measurement of very small surface waves (less than 5 mm) has long been a problem, since the error due to meniscus effects connected with usual probe methods (e.g., resistance, capacitance or electrical contact probes) is of the same order of magnitude as the amplitude. (See (59) and (65).) Thus, an original optical technique was developed. This made use of the effect of a waved surface on transmitted light due to refraction. The method was suggested by the ripple tank technique for qualitatively viewing water wave motions (48, 54) which makes use of transmitted light. Before going into the experimental details, a theoretical description of the wave surface optics is presented.

Assume sinusoidal waves on the surface so that at any time

$$y = a \sin (2\pi x/\lambda) \qquad (3\text{-}1)$$

where y is the elevation of the wave above the mean surface, a is the amplitude (i.e., 1/2 the crest to trough distance), λ is the wave length and x the wave generation direction distance variable. Let α be the tangent angle at a point on the surface; i.e.,

$$dy/dx = \tan \alpha \quad . \qquad (3\text{-}2)$$

Consider a vertical light ray coming up through the liquid and passing through the surface. By trigonometry, as seen in Figure 1, θ_i the angle of incidence (with the normal to the surface) is equal to α. Hence

$$dy/dx = \tan\theta_i = 2\pi m \cos(2\pi x/\lambda) \qquad (3\text{-}3)$$

where m is a/λ. Now for angles less than 10 degrees, the sine function is approximately equal to the tangent. By Snell's Law (22) the refractive index, n is given by

$$n = \sin \theta_r/\sin \theta_i \qquad (3\text{-}4)$$

where θ_r is the angle of refraction with the normal. For θ_r less than 10 degrees (corresponding to m less than 0.02)

$$n = \tan \theta_r/\tan \theta_i \quad . \qquad (3\text{-}5)$$

From Figure 1, it is seen that the angle γ made by the

emergent light ray with the vertical is equal to $\theta_r - \theta_i$. Let δ be the x direction displacement of the light ray from its surface position at a height B above the mean surface. Then

$$\delta/B - y = \tan(\theta_r - \theta_i) = (\tan\theta_r - \tan\theta_i)/(1 + \tan\theta_r \tan\theta_i)). \quad (3\text{-}6)$$

Since y is very small compared to B it can be neglected. On substitution from (3-5) and (3-3)

$$\delta/B = ((n-1)2\pi m \cos(2\pi x/\lambda))/(1+4\pi^2 n m^2 \cos^2(2\pi x/\lambda)). \quad (3\text{-}7)$$

For the water-air system at 25°C the value for n is 1.333 and for m less than 0.02 the second term in the denominator is negligible compared to 1. Thus,

$$\delta/B = (0.666)\pi m \cos(2\pi x/\lambda) \quad . \quad (3\text{-}8)$$

Now consider the case of many uniformly distributed vertical rays coming up through the surface. Each ray can be treated in the manner just described. The wave surface increases the intensity of light passing through the crest half of each wave and decreases the intensity through the trough half. This produces the already mentioned ripple tank effect (48, 54).

A typical plot of light intensity vs. x direction at a height B (less than B_c as described below) is given by Figure 2. The straight horizontal line represents the uniform light intensity (arbitrarily taken as zero) due to a flat (no wave) surface. If the total light transmission is the same for both the flat and waved surface, the area between the curves

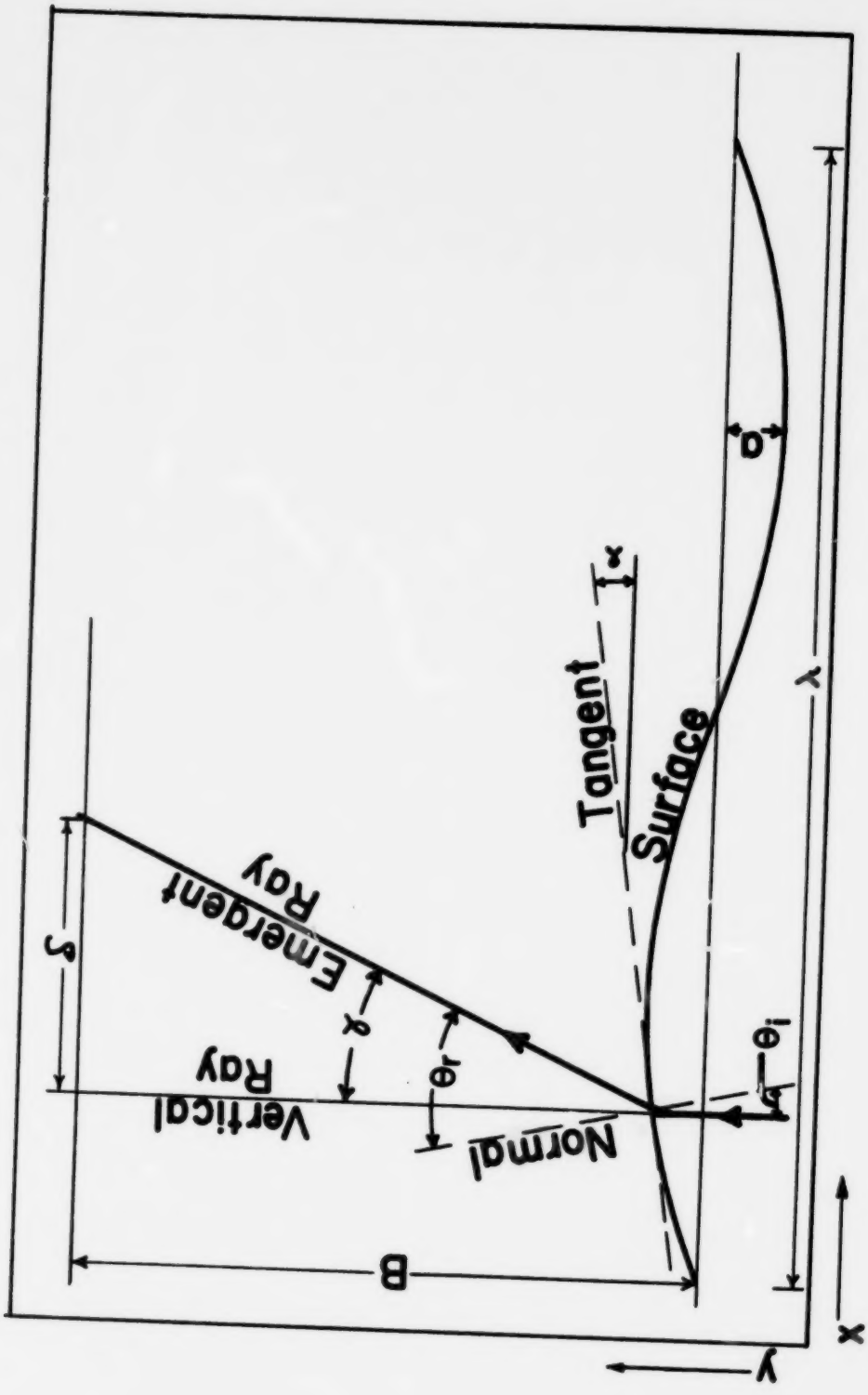

Figure 1 - Schematic Wave Diagram

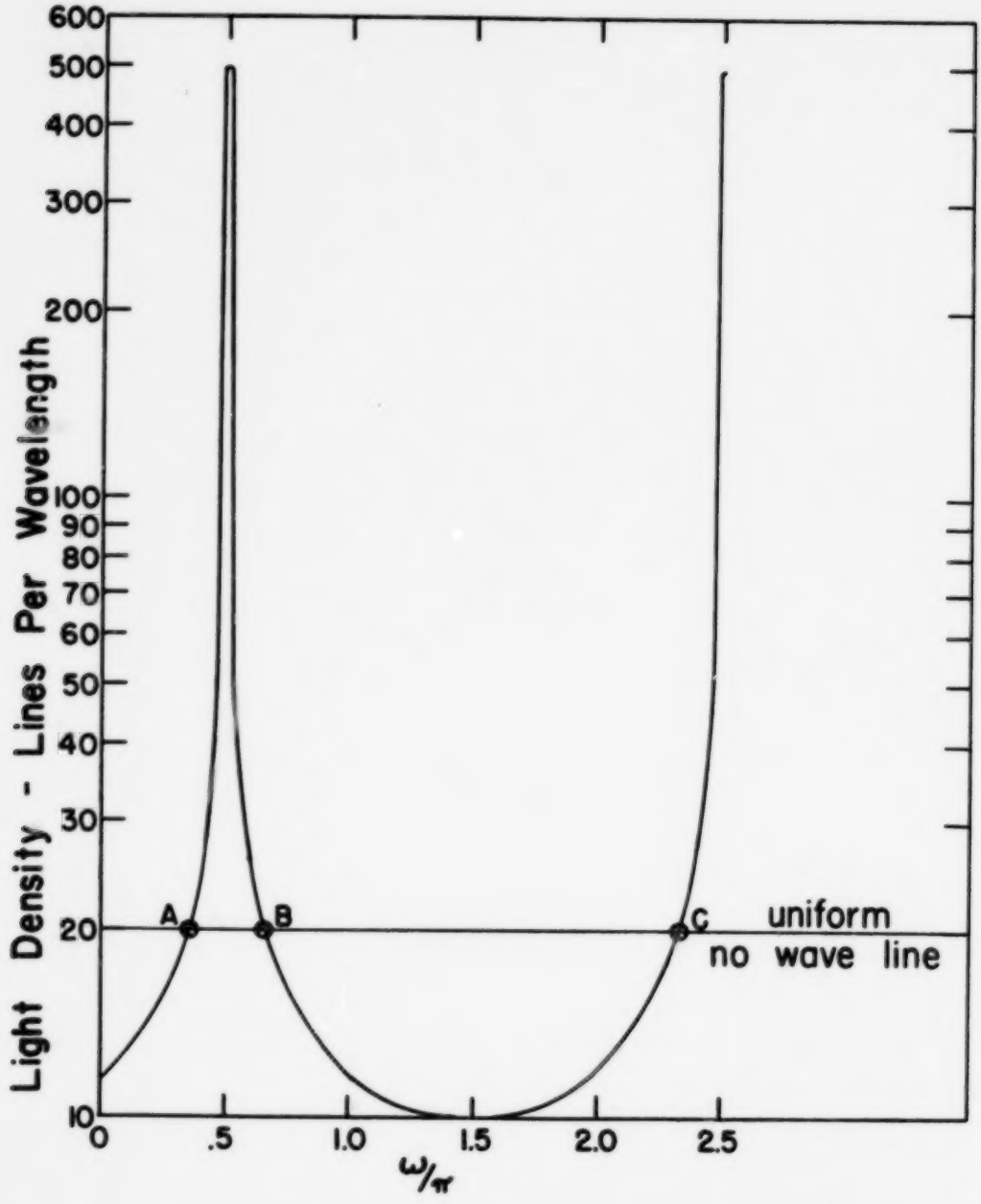

Figure 2 - Light Intensity Pattern

Figure 3. Wavelength Measurement, 500 CPM

in the interval AB must equal that in the interval BC. Furthermore, it is seen that the points A, B and C are node points (i.e., $2\pi x/\lambda$ is equal to 0 or π at these points). For the node points (Cos $2\pi x/\lambda$ is equal to $\pm$ 1), (3-8) becomes

$$\delta/B = \pm (0.666)\pi/m \quad . \tag{3-9}$$

Let B_c be the height above the surface of the intersection of rays going through 2 consecutive node points that bound a wave crest. For this case,

$$\delta = \lambda/4 \quad , \tag{3-10}$$

considering only the case of δ positive. Substituting into (3-9)

$$B_c = \lambda/2.664\pi m \quad . \tag{3-11}$$

For the cases of B less than or equal to B_c, let d be the distance between two node point rays at height B (i.e., distance AB on Figure 2).

$$d = 2(0.25\lambda - \delta) \quad . \tag{3-12}$$

Let S equal d/λ and let L equal B/λ. Then upon algebraic rearrangement

$$m = (0.5 - S)/4.18L \quad . \tag{3-13}$$

This relationship gives the amplitude as a function of "screen height" B and the "band width distance" d, which are

both measurable. It should be emphasized that this holds only for B less than B_c. Detailed analysis indicates the existence of a point of sharp concentration of crest rays below B_c. This is due to the top of the crest approximating an arc of a circle. If B is taken near this point of sharp concentration, B will be below B_c.

The above treatment assumed m to be less than 0.02. If in practice this condition did not hold, the equating of tangent to sine is no longer valid and a simple analytical expression for m is not attainable. However, by use of Snell's Law and the trigonometry of the situation a trial and error numerical solution can be used to calculate m from B and d. The node point rays can still be used as above, since justification of their use is not dependent on the value of m.

The experimental method based on the above is now described. With the wave generator in operation, an electronic flash unit (rated at 1/1500 second) placed below the ripple tank sent a flash of light through a small transparent area in the tank and up through the liquid. The image of the light at a given height above the surface was focussed on a ground glass screen and photographed. The flash unit was synchronized with the camera and was at a sufficient distance below the surface so that light rays going through the exposed area were essentially vertical. Covering all but a small circular area on the face of the flash unit, made it essentially a point source of light. Experimental details are

discussed below.

The distance of the ground glass screen above the wave surface corresponded to B. The negative image of the photographed light pattern was magnified by a film strip projector. A photometer was used to scan the projected image and determine the (negative) light intensity pattern. This was compared to a photograph taken similarly for the no wave (flat surface) case. The band width d was then determined by noting the distance between node point rays (where the intensity of the two patterns are equal). The hydrodynamically determined wave length (see section C below) was used to scale the measured distances to actual size and then amplitudes were calculated by (3-13). Figure 6 shows typical light patterns printed as photographic positives.

B. Description of Experimental Equipment

1. Ripple Tank. The inner dimensions of the plexiglass tank used for these studies were 20 inches long 6 1/4 inches wide and 4 inches deep. It was designed to operate with a 2 1/4 inch liquid depth. Both ends were fitted with gauze enwrapped metallic screening which served to damp out wave motion and prevent reflection.

The wave generator consisted of 25 rigidly supported vertical stainless steel rods (diameter of 0.053 inches) placed 1/4 inch apart. This assembly moved up and down to create waves, but was otherwise restricted by being set in grooves notched out of the side of the tank. The generator

was at the center of the tank (with respect to length) so that waves were generated from the center towards both ends in a symmetrical manner. Each rod produced a circular wave which upon interaction produced a two dimensional wave train.

The generator assembly was driven by two 3/4 inch diameter, 1/8 inch offset cams on a shaft, belt driven from outside by a Master Speed Ranger variable speed drive and motor. This gave a total vertical travel of 1/4 inch. The cam shaft and spring mounting of the generator along with the shaft seal were all contained in a 2 by 3 inch plexiglass section attached underneath the tank at the center. This section was separated from the main chamber by plexiglass plates, but with sufficient clearance for the generator assembly movement. The partition was present to minimize the effect of fluid motions created by the cam shaft on the main chamber. Figure 4 is a photograph of the tank and motor showing the rod assembly and drive belt.

2. Amplitude Measuring Equipment. The ripple tank described above was supported on the upper level of a wooden stand with the flash unit light source on the lower level. This provided for a light source to tank base distance of 51 inches. A 2 inch by 1 inch field of light was produced by inserting an opaque plate with the field rectangle cut out, underneath the tank. The point light source was lined up with the center of the field, so that the maximum deviation from the vertical of light rays reaching the liquid was

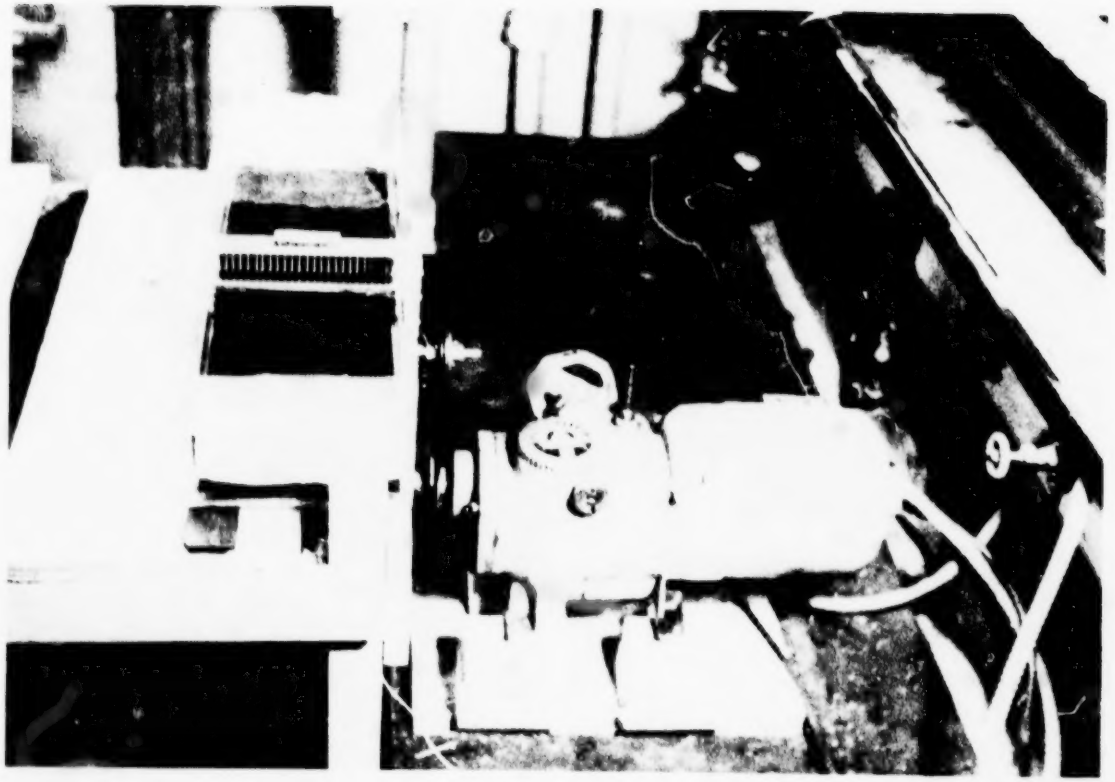

Figure 4. Ripple Tank

arctan. (1/51) which is equal to 1.06°. Refraction of the light from air to plexiglass to water slightly decreases this deviation though the rays become somewhat displaced.

The emergent light image was captured on a ground glass screen, which constituted the bottom of an otherwise black box open at the top. This box was attached to a vertically moveable gear device so that the height of the screen could be changed and measured. Also attached was a camera support, mounted so that the special lens attached to the camera was always 170 mm (the focal length of the lens) above the screen. The camera shutter was synchronized with the light source by means of a long extension cord. Figure 5 shows the support stand, ripple tank, light source, screen and shadow box camera and the height adjuster.

As previously mentioned, the light pattern photographs (e.g., Figure 6) were analyzed by a photometer. Each negative picture was projected onto a horizontal surface so that it was magnified about 1.8 times the actual size. The photoelectric cell of the photometer, fitted with a 0.01 inch aperature, could be moved along a calibrated slide along this surface and positioned to 1/32 inch. By slowly moving the cell in the direction corresponding to wave generation and noting the voltage density scale readings, the light density pattern (actually film density) was determined.

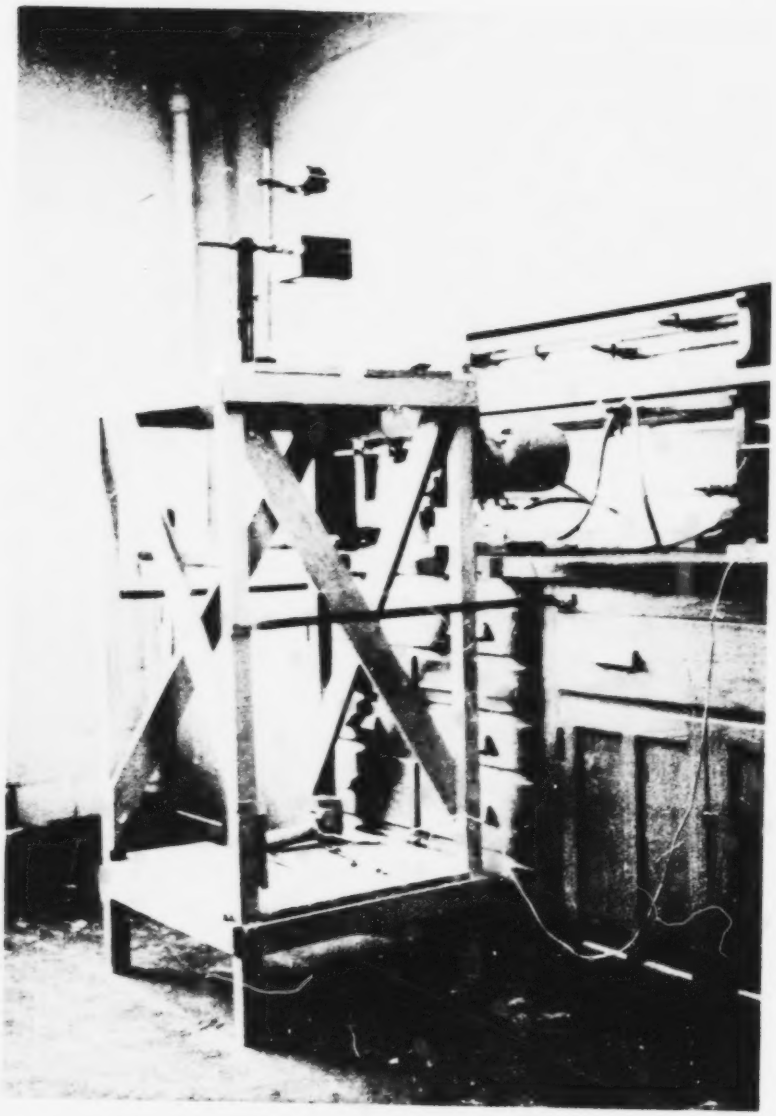

Figure 5. Amplitude Measuring Equipment

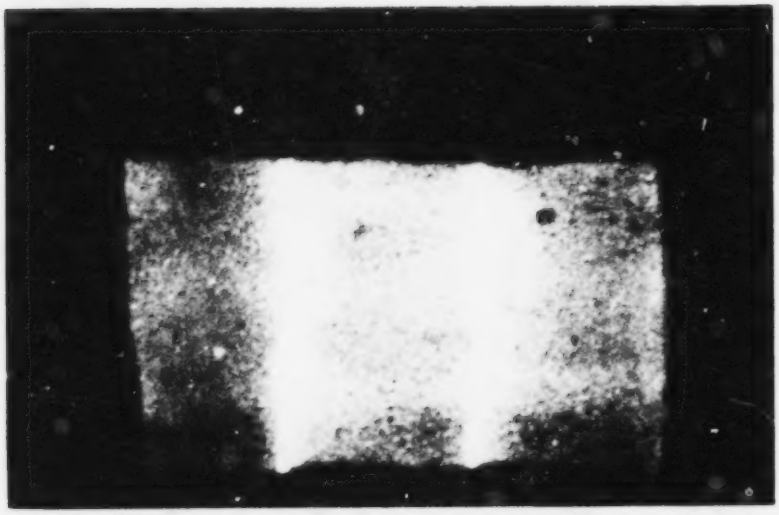

(a)

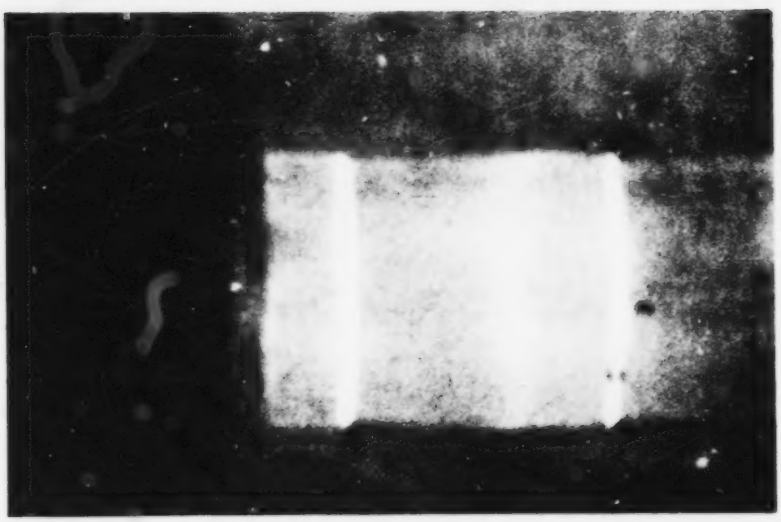

(b)

Figure 6. Typical Light Pattern Photographs (positives)

C. Experimental Results and Discussion

1. Wave Length and Frequency Correlations. A series of frequency and corresponding wave length measurements using the methods of Section A, are presented in Figure 7. The solid curve of this plot represents the hydrodynamic relationship

$$(f\lambda)^2 = (g\lambda/2\pi + 2\pi\sigma/\rho\lambda)\tanh(2\pi h/\lambda) \qquad (3\text{-}14)$$

(See Coulson (16).) for water at 20°C. Because of the good fit of the data with this apparatus to this relationship along with the experimental experiences of previous workers (e.g., (12)), it was decided to measure only frequency in future (mass transfer) experiments. (3-14) would then be used to determine wave length.

2. Amplitude Data. Data and calculated amplitudes taken at 5 different frequencies are presented in Table A-1 (Appendix). Different screen heights were used for many of the similar position data points, to show reproducibility of the method. Figure 8 is a plot of reciprocal amplitude vs. tank position (distance from the generator). The ordinate was so chosen because a method of least squares straight line fit for each frequency indicated y intercepts close to the reciprocal of half the vertical cam travel. This is the expected value of amplitude at the generator. The straight lines shown on Figure 8 are derived by setting the intercept at this value (3.15 cm^{-1}) and applying the least squares

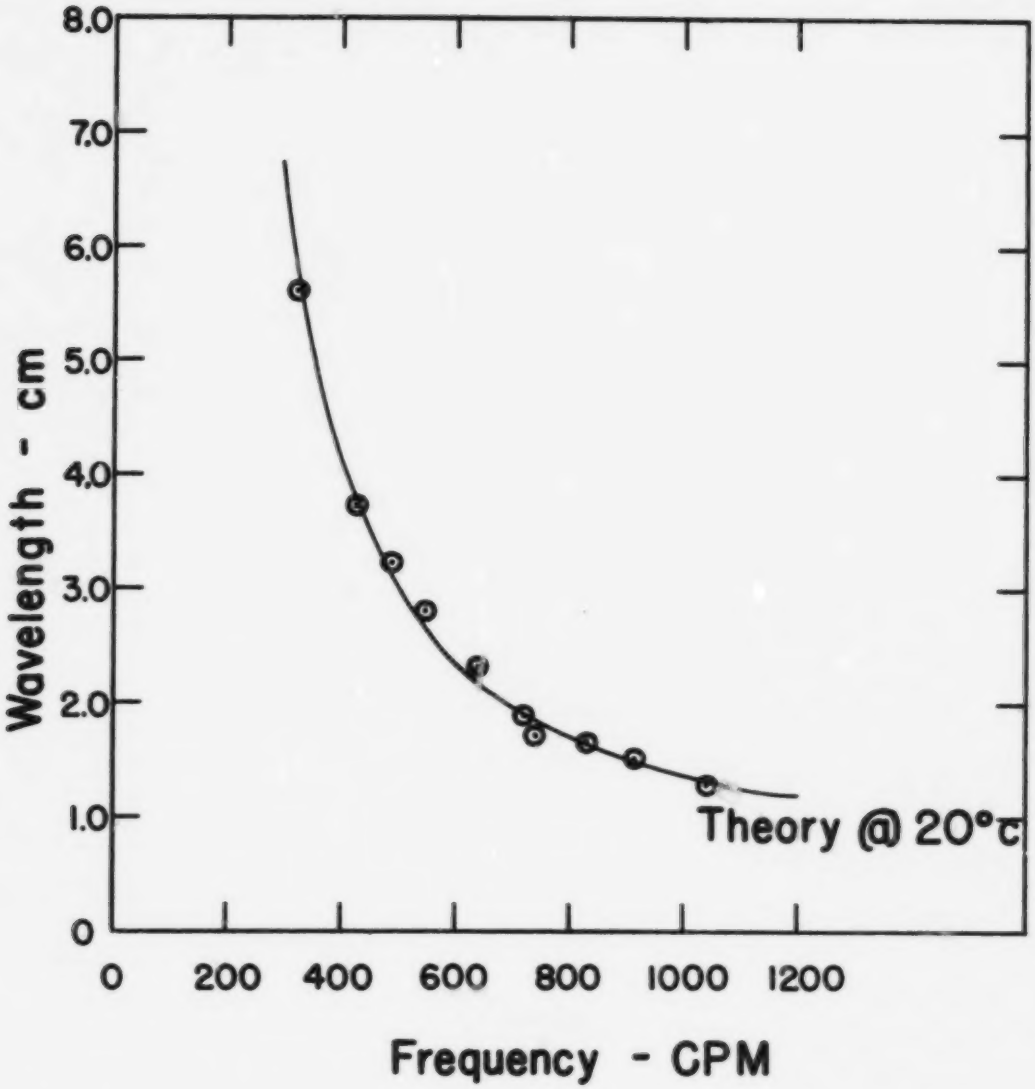

Figure 7 - Wavelength vs Frequency For Water

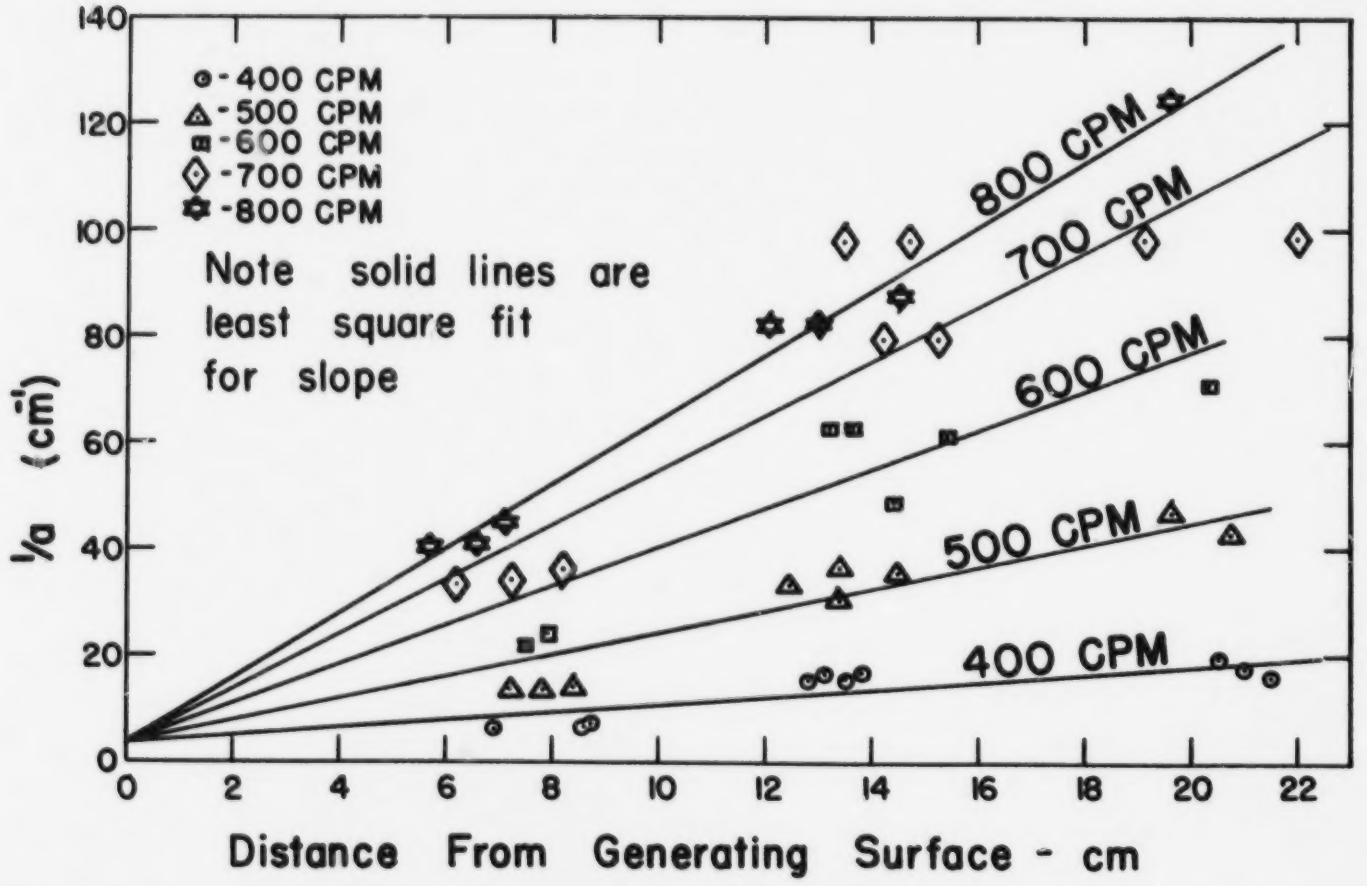

Figure 8 - Reciprocal Amplitude vs Distance From Generating Surface

method to determine the slope. From this, empirical correlations of the form

$$a = 1/(\epsilon x + \beta) \qquad (3\text{-}15)$$

are obtained. Table 3-1 lists values for ϵ and β determined for each frequency. Figure 9 shows a plot of amplitude vs. frequency at various positions based on the smoothed data.

Three significant sources of experimental error were apparent in carrying out these experiments. The first was the presence of additional unexpected light bands in the light pattern pictures. An example of such light is seen in Figure 6b between the two bright bands. It is believed that these bands are due to secondary motions on the surface. This conclusion was supported by the observation of virtually no such additional bands when a piece of cloth screening was suspended into the liquid, about 1/2 inch from the generator. This is a known method of eliminating secondary wave motions. By adjusting screen height so that sharp bright primary light bands are obtained, these bands are easily distinguished. However, the presence of the secondary effects on the surface somewhat disrupts the assumed light refraction model. Hence, it is a source of error.

The second error source was the non-uniformity of no wave "null" pictures. This was in part due to lens distortion and also to optical non-uniformities in the plexiglass base through which the light passed. It was assumed, however, that these effects were present for both wave and null pictures.

TABLE 3 - 1

CONSTANTS FOR EQUATION (3-15)

Frequency (CPM)	ϵ (cm^{-2})	β (cm^{-1})
400	0.765	3.15
500	2.08	3.15
600	3.75	3.15
700	5.16	3.15
800	6.06	3.15

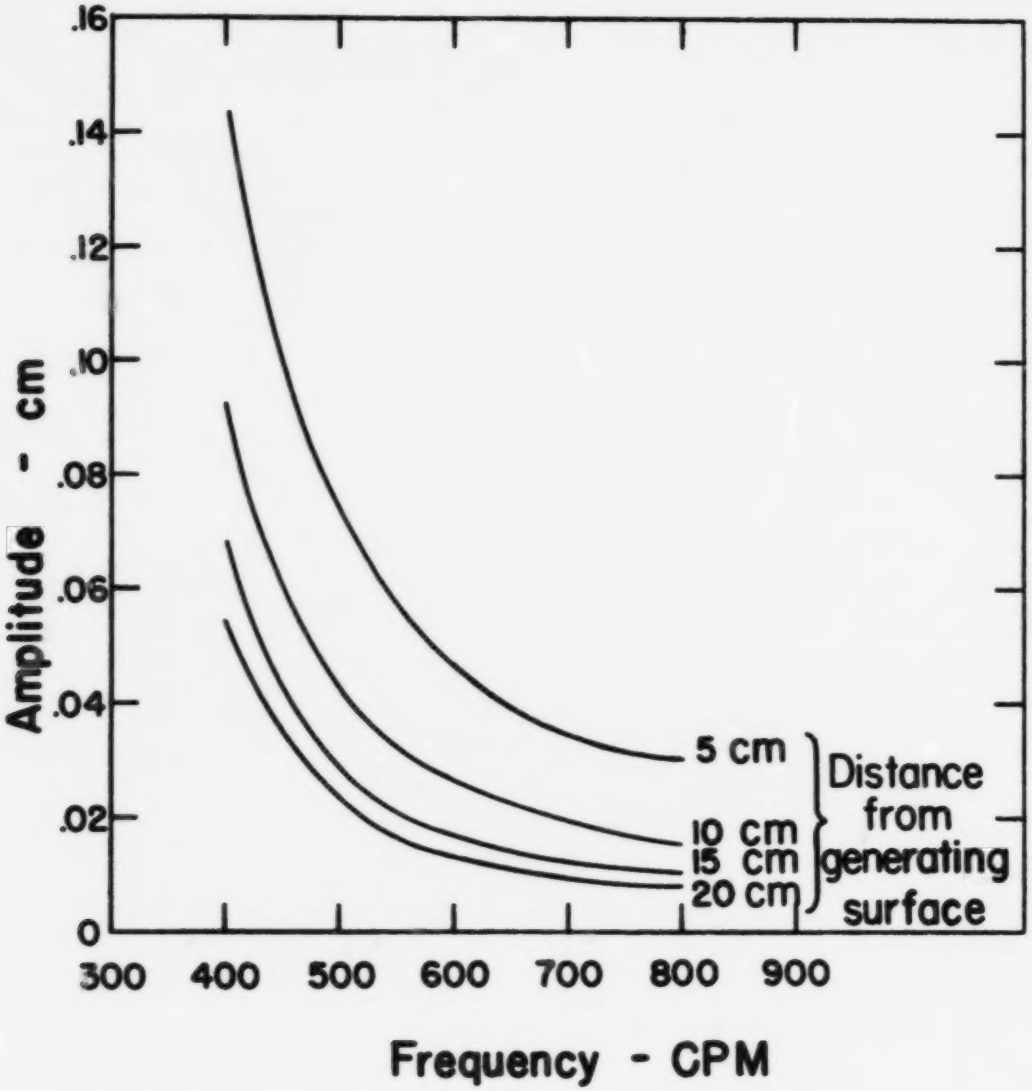

Figure 9 - Amplitude vs Frequency

The error was, therefore, minimized. Only a short length of the null picture had to be measured to correspond to each short sharp bright band of the wave picture. The null pictures were reasonably uniform over such short distances. A third error source resulted from difficulty in exactly positioning each wave picture so that it corresponded to the equivalent null picture when projecting the light pattern pictures. This is actually another result of the non-uniformity of null pictures.

CHAPTER IV

MASS TRANSFER EXPERIMENTS

A. General Remarks

The objective of the work described in this section was to obtain sets of experimental data that would demonstrate the effect of surface waves of different frequencies on absorption. Furthermore, the data was to be of such a form as to lend itself to the types of analysis found in other sections of this dissertation.

Four gas-liquid systems were chosen for study. They were:

1. Oxygen-Water
2. Helium-Water
3. Carbon Dioxide-Water
4. Propylene-Water.

In all cases the direction of mass transfer was from the gas phase to the liquid. The gases were used as supplied by the manufacturer and in all cases contained less than one per cent impurities. The gas from the cylinder was saturated with water vapor to eliminate interphase water transfer. The liquid water phase was initially deaerated so as not to contain any of the gas being studied or other components that could potentially interfere with mass transfer.

Water was the liquid phase in all cases. Its advantage lay in the availability of experimental data on solubility and diffusivity (for dilute solutions) for a significant number of gaseous elements and compounds. Furthermore, wave hydrodynamics have been well established both theoretically and experimentally for water.

The four gases were selected so that an extended range of equilibrium solubilities and diffusivities in water could be observed. Since, by their nature, all the systems involved dilute aqueous solutions, the variation in diffusivity directly influenced the dimensionless Schmidt Number. Table A-2 of the Appendix presents solubility and diffusivity values for the four systems as reported in the literature. The diffusivity data was that measured and compiled by Vivian and King (60). In this recent article, these investigators have reviewed the earlier data along with data of their own. It was felt that the diffusivity values which they recommend are the best available. The International Critical Tables (26) served as the primary source of solubility data. In order to extend the solubility data for Propylene-Water into the experimental temperature range, supplementary data was obtained from the Master's Thesis of Azarnoosh (2).

The general experimental scheme was to measure the total amount of gas absorbed in the water as a function of time in an unsteady state (non-flow) experiment. This was started with a given amount of water containing none of the transferring component. Such experiments were carried out with no

waves and with waves of different frequency on the liquid surface. Details of experimental procedure are given below.

The unsteady state scheme was used because the experimental techniques and wave hydrodynamics could be simplified when compared to alternate steady state flow situations. The major simplification was the elimination of chemical analysis. Since steady state systems would have involved small solute differences of dilute solutions, such analysis would have posed considerable experimental difficulty. However, for the unsteady state case it was sufficient to measure the pressure, volume and temperature of the sealed gas space as a function of time and from this calculate the quantity of gas absorbed. The runs were made under ambient conditions and it was felt that the ideal gas law was adequate for this calculation. Since the gas had already been saturated with water at room temperature, no water evaporation or condensation occurred. Therefore, the change in quantity of gas was entirely due to absorption.

Two dimensional progressive waves were produced for all the wave runs and the principal frequencies used were 400, 600 and 800 cycles per minute. This range resulted from experimental considerations. Below 400 CPM, wave lengths of the order of liquid depth result and assumptions involved in the wave hydrodynamics are no longer valid (See Chapter II). Three dimensional turbulent wave motion was observed at frequencies above 1000 CPM. Also prohibitive equipment stresses

occur at high frequencies.

B. Equipment and Procedure

1. Deaeration of Water. Laboratory distilled water was deaerated before use in mass transfer runs. The apparatus consisted of a heating vessel, a storage vessel and a circulating system motivated by a small centrifugal pump. Figure 10 shows this arrangement schematically. The heating vessel which was at the highest elevation contained a 2250 watt immersion heater connected to a 110 volt AC source. Water flowed down from this vessel through the circulating pump, then up through the storage vessel and back into the heating vessel. Valves for trapping water in the storage vessel were provided. This container was jacketed to allow rapid cooling (using cooling water). The capacity of the two vessels plus circulating lines was about 5 gallons, with the storage vessel holding about 2 gallons. This quantity exceeded the water requirement for a mass transfer run.

The procedure for deaerating water was as follows. The system was charged such that both vessels and all circulating lines were full. Circulation was started with valves B and C closed and valves A and D open (See Figure 10). Next power was supplied to the immersion heater in the heating vessel. The water was allowed to circulate and heat for 3 hours. The time required to bring the water in the heating vessel to its boiling point was approximately 1.25 hours, so that boiling occurred for 1.75 hours. During that time about

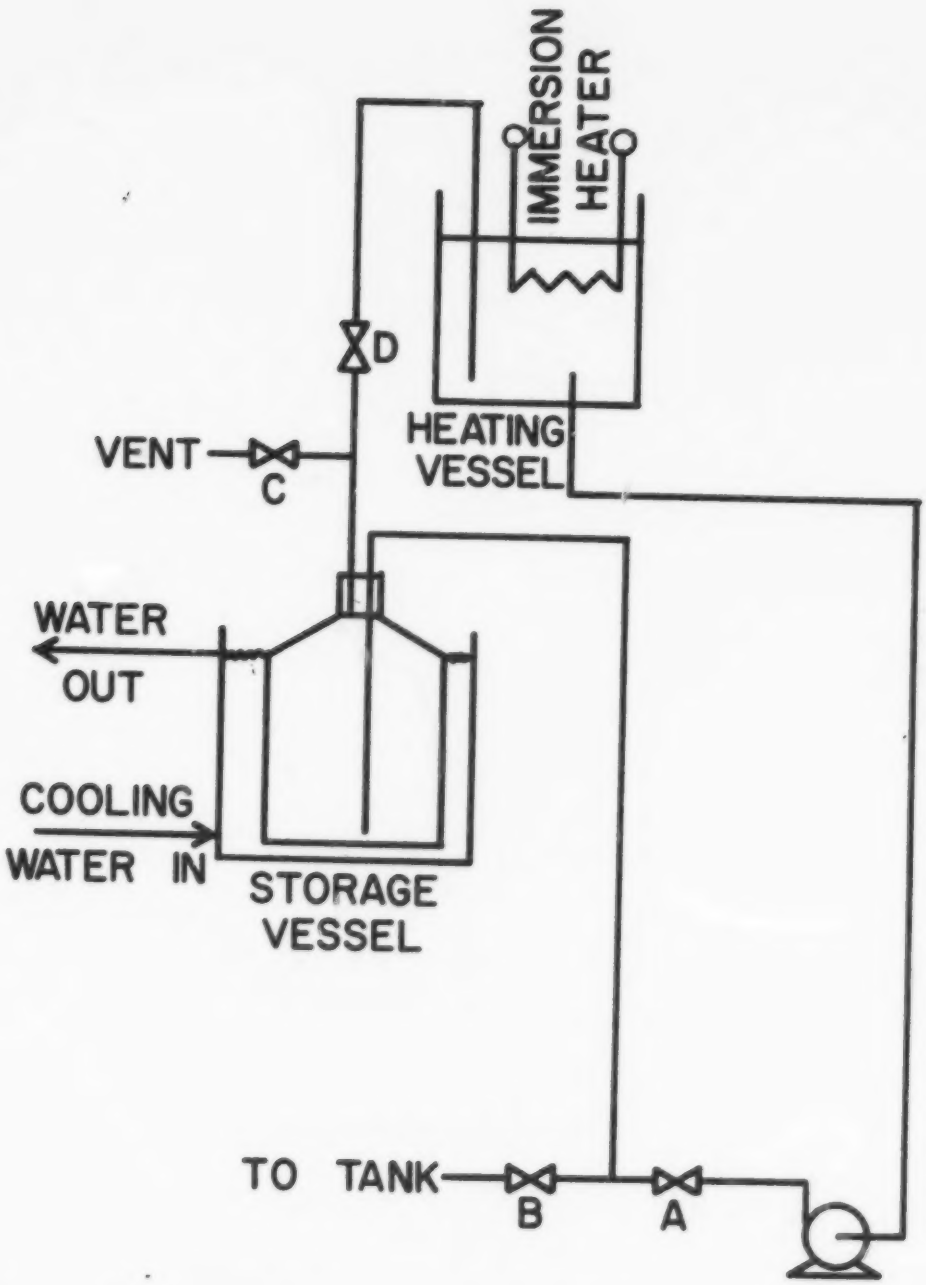

Figure 10. Water Deaeration Equipment

1 gallon of water boiled off from the open heating vessel. The circulation rate was approximately 0.3 gallons per minute. Upon completion of the heating cycle, valves A and D were closed and the circulating pump and heater shut down in that order. The water, deaerated by boiling was trapped in the sealed space between the four valves, which included the storage vessel. This water was then cooled for use in the mass transfer runs. The process was repeated before each run.

2. Water Saturation of the Gas and Purging of the Tank. Before each run the wave tank was emptied and dried with compressed air. The gas being studied was then passed from its storage cylinder through a water saturater and then purged through the tank. This was done for 2 hours at a gas flow rate of about 0.05 SCFM. The saturater consisted of a scintered glass sparger immersed in distilled water. A qualitative test for saturation was made by placing a wet bulb thermometer close to the throat of a nozzle through which the wet gas was flowing. In all cases no observable drop in temperature was noticed. This same test repeated with dry cylinder gas produced a temperature drop of over 20°F for all cases. The purging lines were all of copper tubing. The gas entered and vented through ports atop the tank. After the purge, the tank containing the saturated gas was sealed by closing the valves on the entry and vent lines.

3. Mass Transfer Equipment. The principal apparatus for mass transfer studies was a sealed ripple tank. The wave generation and damping mechanisms as well as the shape and major dimensions of this device were given in the previous chapter. Briefly summarized, waves were generated by a series of parallel vertically moving rods which could be driven at varying frequencies by a motor drive coupled to a cam mechanism. This created circular progressive wave pattern for each of the rods which quickly interacted to give a two dimensional wave front moving down the rectangularly shaped tank. At the ends of the tank gauze enwrapped metallic screening was used to damp out the waves and prevent reflection.

A number of important modifications and additions were necessary to adopt the ripple tank for mass transfer. Figure 11 should be referred to for a graphical description of the experimental layout.

Whereas the previously described wave property measurements were made with an open ripple tank, it was necessary to seal the tank during absorption experiments. Thus measurements of pressure, volume and temperature (P-V-T) could be used to monitor the change in gas quantity. A 1/2 inch thick aluminum top plate was attached to the tank by means of a #2 Permatex Compound seal along the rim. Since the pressure inside the tank remained essentially atmospheric during operation, the weight of the top plate was sufficient to keep the seal. The sealing compound was of the non-hardening type, so

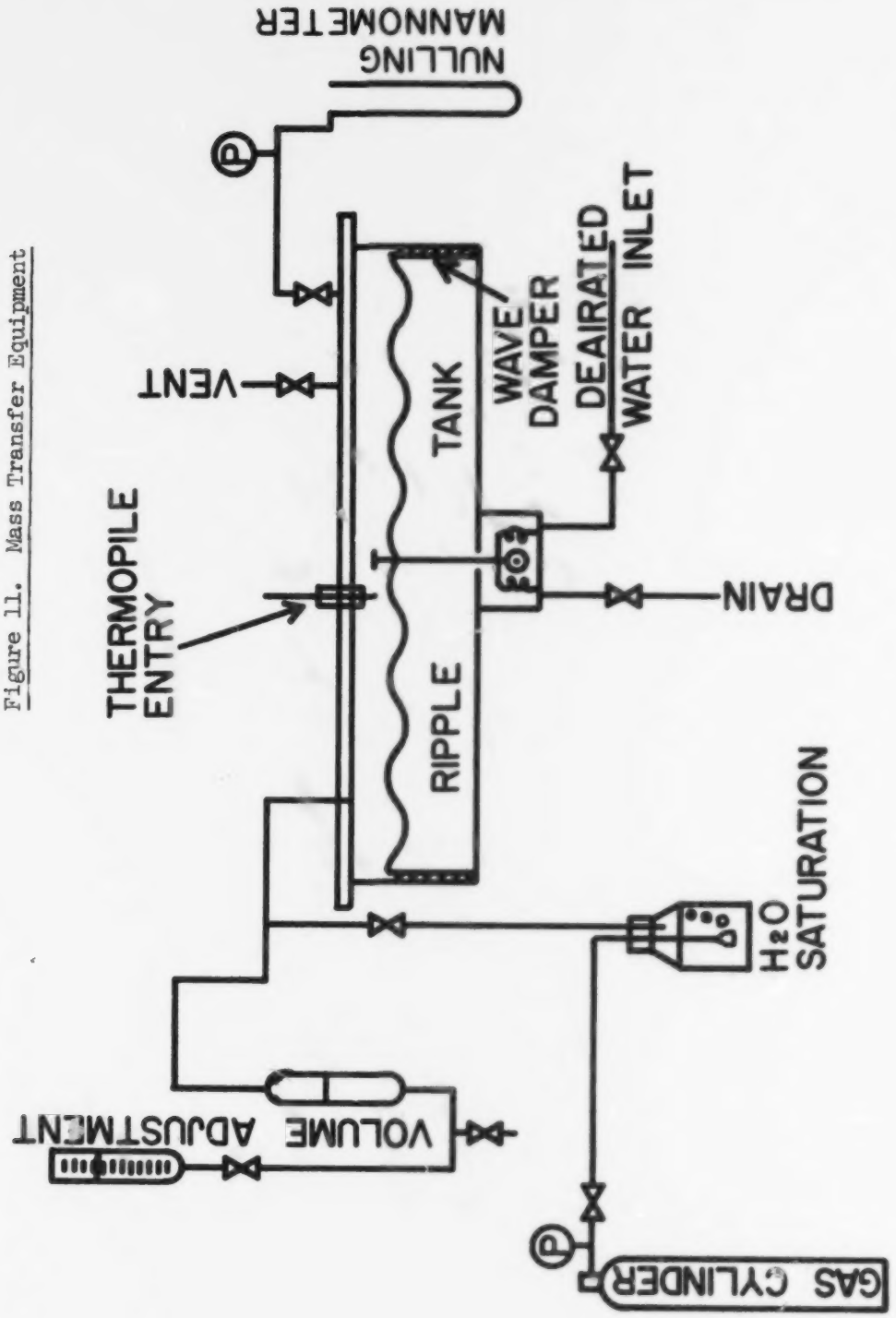

Figure 11. Mass Transfer Equipment

that the top could be removed for maintenance and alterations in the tank. In addition sealing paint was applied to all the seams of the plexiglass portion of the tank.

The gage pressure of the gas space was observed by means of a vertical U-tube mannometer connected by copper tubing to a sensing port on the tank top plate. The mannometer fluid was water already saturated with the gas under investigation. One leg of the mannometer was exposed to the atmosphere. A barometer was available, so that gage pressure readings were corrected to absolute pressure.

Since it was necessary to continually decrease the overall gas volume by small amounts (see procedure below), a volume displacement mechanism was incorporated. This consisted of a burette attached to a needle valve outlet feeding into a U-tube. The U-tube was attached to a 250 ml. glass bulb which in turn was connected by copper tubing to the tank top plate. Thus, the volume of the bulb and tubing was an integral part of the gas volume. (Refer to Figure 11.) The system volume could be decreased by allowing water to slowly flow from the burette into the bulb either continuously or incrementally. The volume change was observed by recording the drop in water level in the calibrated burette. Because of variation in order of the volume change, a 10 cc burette was sufficient for Oxygen and Helium runs while a 250 cc one was used for the two other systems. Since more than 250 cc were absorbed during the Carbon Dioxide runs, a return line was used for transferring water back from the

bulb to the burette for reuse.

The initial gas volume V (including the 250 cc bulb) was determined with air as the gas phase. The tank was charged to the standard liquid level with air-saturated water. The volume was decreased slightly by adding a known volume of water from the burette to the bulb. The air pressure before and after this addition was recorded. This was done isothermally so that

$$P_1V = P_2(V - d) \qquad (4\text{-}1)$$

where P_1 and P_2 are the before and after pressure readings respectively and d the change in volume. V was thus calculated from P_1, P_2 and d. The actual volume at any time during a run was therefore V-B, where B was the overall change in burette volume at that time. The value of V was 4260 cc for Carbon Dioxide and Propylene runs and 2950 for Oxygen and Helium. This latter smaller volume was attained by attaching plexiglass blocks to the tank top plate.

A series connected thermopile consisting of 5 hot and 5 cold copper-constantan junctions was used to detect and measure the gas temperature. The hot junction positions were distributed over the gas volume so as to compensate for any slight temperature differences from point to point. During readings the cold junctions were kept in an ice bath. The EMF generated by the thermopile was measured by a "precision" potentiometer capable of being read to 0.001 milivolts. The standard thermocouple calibration (multiplied by 5) was

used to convert EMF to temperature, since in making P-V-T calculations, accurate temperature difference values rather than absolute temperature values were required.

Both the entry and drain ports for water were at the bottom of the tank. Water flowed from the deaeration storage vessel to the tank by syphon action with a net head of about 4 feet. Using a 3/4 inch diameter tubing line, it was possible to flow in the necessary water for a run within 20 seconds. The standard water level was 2 1/4 inches above the bottom of the tank, which corresponded to a water volume of 4600 cc. A dial thermometer was in the inlet water line.

In making mass transfer runs it was necessary to cool the deaerated water slightly below ambient temperature just before each run. Otherwise, the water temperature could be slightly higher than that of the gas upon entering the tank. It was observed that under this condition small water droplets formed on the sides of the tank gas space, increasing the mass transfer surface area and hence the absorption rate.

4. Mass Transfer Run Procedure. The details of operation for a mass transfer run are given below. They are presented in the form of an operating instruction manual. This is helpful, since the actual order of operations is clearly described. Before each run water was deaerated and the tank dried and purged as previously described. The specific steps follow.

a. Record initial tank gas temperature.

b. Introduce deaerated water into tank by opening valve C and then valve B (Figure 10) so as to allow syphon action. While the water flows in, the vent valve is open so that no pressure buildup occurs. When the desired liquid level is reached close valve B and the vent valve. Record inlet water temperature.

c. Immediately start wave generator motor and stopwatch. For no-wave runs, of course, the generator is not started.

Note. The total time taken for steps b and c was about 20 seconds.

d. Allow an initial time of 25 seconds for Propylene and Carbon Dioxide or 100 seconds for Oxygen and Helium, for the system to reach a hydrodynamic steady state. Then open and close the vent valve quickly and take initial temperature and barometric pressure readings. The initial gage pressure is, therefore, zero (null).

e. As the run proceeds the gas phase gage pressure will tend to decrease because of absorption. Throughout the run compensate for this drop by means of the burette and bulb volume adjustment mechanism. In this manner keep the gage pressure as close as possible to zero; i.e., decrease the total gas volume such that the gas remains at atmospheric pressure.

Note. The advantage of this pressure adjustment method was twofold. First, since the pressure remained constant, there was no variation in equilibrium saturation gas

concentration due to pressure changes. Secondly, by minimizing the pressure driving force between the contained gas and the atmosphere, the error producing possibility of leakage was minimized. Due to the relatively slow rates for Helium and Oxygen, incremental volume adjustment was necessary for these systems. Continuous adjustment was effected in the other two systems.

f. Throughout the run, check the wave frequency by means of a stroboscope light directed on the generator drive shaft. Adjust the variable speed drive if necessary.

Note. In practice such adjustment was seldom required, since the drive mechanism performed well. Among the wave properties, only frequency was checked since the results of previous work relate amplitude and wave length to frequency (See Chapter III).

g. At various times during the run, take data. Record the time elapsed, gas phase temperature and barometric pressure. The gage pressure should be nulled (zero) whenever data is taken. Also record the burette level.

h. At the conclusion of the run, take a final set of data, withdraw a water sample and measure its temperature. Then adjust the drive frequency (RPM) to the value desired for the next run and then shut off the motor. Drain and dry the tank for the following run.

In summary, Table A-3 in the Appendix lists the operating specifications for mass transfer runs.

C. Presentation of Data

The data as presented in Tables A-4 to A-7 of the Appendix, shows the total quantity of gas absorbed as a function of time. As an alternative, it could have been presented on a moles absorbed per unit of surface area or moles absorbed per unit of liquid volume. These representations would have been misleading, however, since the flux probably was not uniform over the surface due to amplitude attenuation. Furthermore, the unsteady state runs indicate a concentration gradient with depth, rather than a uniform concentration of solute throughout the liquid volume.

The values of Tables A-4 to A-7 were calculated from primary P-V-T measurements of the runs. The quantity absorbed was arbitrarily set at zero for the time corresponding to the first reading. Thus, the actual mass of gas absorbed at any time is somewhat higher due to the amount absorbed between the initial moment of gas liquid contact and the first reading.

Special runs wherein the water was saturated with air prior to running, were made with the Carbon Dioxide and Helium systems. In addition a run in which the water inlet time was purposely delayed to 8 minutes was made with Carbon Dioxide. The former were run to qualitatively assess the effect of interaction of already dissolved air on mass transfer, while the latter tested the effect of initial inlet water turbulence.

CHAPTER V

ANALYSIS AND DISCUSSION

A. Data Analysis

The data are presented in terms of tabulations of total gas absorbed with corresponding time for each of the runs (See Chapter IV).

Prior to the discussion, it is noteworthy to make some general remarks on methods of calculation. The values of C_i, the equilibrium concentration of the gases in water, are determined at the average gas temperature of the run from the Henry's Law constants of the International Critical Tables (26), supplemented by other Propylene-Water data (2). The dimensionless groupings, discussed in this chapter are calculated from the values of properties at atmospheric pressures and the average gas temperature of each run. The values for molecular diffusivity are generally only given at one temperature (usually 25°C). Temperature corrections for diffusivity are made by keeping the quantity $D\mu/T$ constant for each system, as suggested by Vivian and King (60).

1. Initialization Error. An initialization experimental error results from the fact that the first phase contact occured before wave generation or timing was started. In practice, the

time error involved here was about 20 seconds. However, due to the introduction of water into the tank and starting the wave generator, transient behavior for some time thereafter is expected. The "delayed time of water addition" run made for the no wave Carbon Dioxide system showed the time error due to filling to be small. In this run, the behavior of "gas absorbed vs. time" was reproduced even though there was a time displacement.

A more significant error was due to the lack of temperature equilibrium at the start of a run, caused by deliberate subcooling of the liquid. The necessity for this action was discussed in Chapter IV. A definite time interval was necessary to achieve temperature equilibrium between the liquid and gas as well as between the gas and the thermocouples. Since calculation of the total gas absorbed quantity is dependent on the temperature (P-V-T calculation), this had a direct effect on the early time data. This was especially true for the very sensitive Oxygen and Helium systems. Reproducibility of short time behavior was poor for these.

Due to the initialization errors discussed above, only data for times of 15 minutes (900 seconds) or greater are considered. This is probably overly conservative for the Carbon Dioxide and Propylene systems. The limitation is, however, applied to all four systems so as to standardize inter-system comparisons based on the data.

2. Data Plots. As suggested by equation (2-68) of Chapter II, the data was plotted in the form of $Ln(1-\Delta n/C_i V_L)$ vs. time for all runs. By applying the criteria that the ratio $D_w \pi^2 \theta/4h^2$ be equal to or greater than 0.1, it was determined that equation (2-68) and the above plots could be used to calculate D_w for all of the driven runs from the data points corresponding to times in excess of 2400 seconds. In addition, the no wave runs for Helium and Carbon Dioxide could also be analyzed in this manner.

For the no wave Oxygen and Propylene runs, it was necessary to use the infinite depth assumption, of Chapter II, to calculate D_w since the $D_w \pi^2 \theta/4h^2$ ratio was less than 0.1 for all the time values of these runs. Thus, by equation (2-76), D_w was calculated from the slope of plots of Δn vs. $\theta^{0.5}$.

Plots of $Ln(1-\Delta n/C_i V_L)$ vs. θ for the applicable cases are presented by Figures 12 through 16. Figures 17 and 18 are the plots of Δn vs. square root of time for no wave Oxygen and Propylene. Runs with insufficient significant (over 2400 seconds) data points are ommited. The values of D_w, calculated from the slopes of these curves are listed in Table A-8 of the Appendix. This table also gives the values of some dimensionless groups, the use of which is discussed further on in this chapter. These include the ratio D_w/D, the effective to molecular diffusivity ratio.

3. Mass Transfer Coefficient. Visual examination of plots of Δn vs. θ, indicates a straight line correlation may

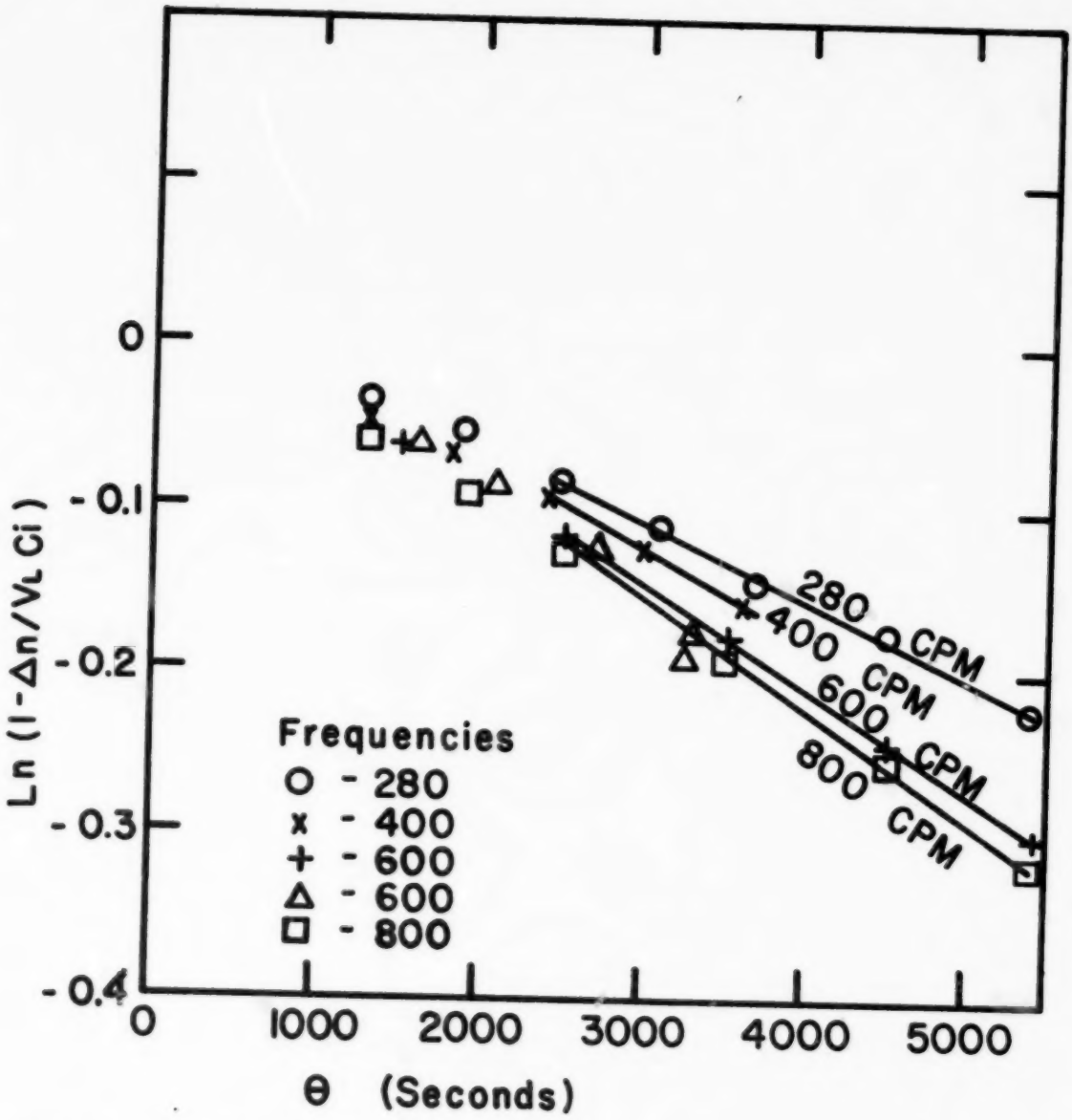

Figure 12. Oxygen Absorption With Waves

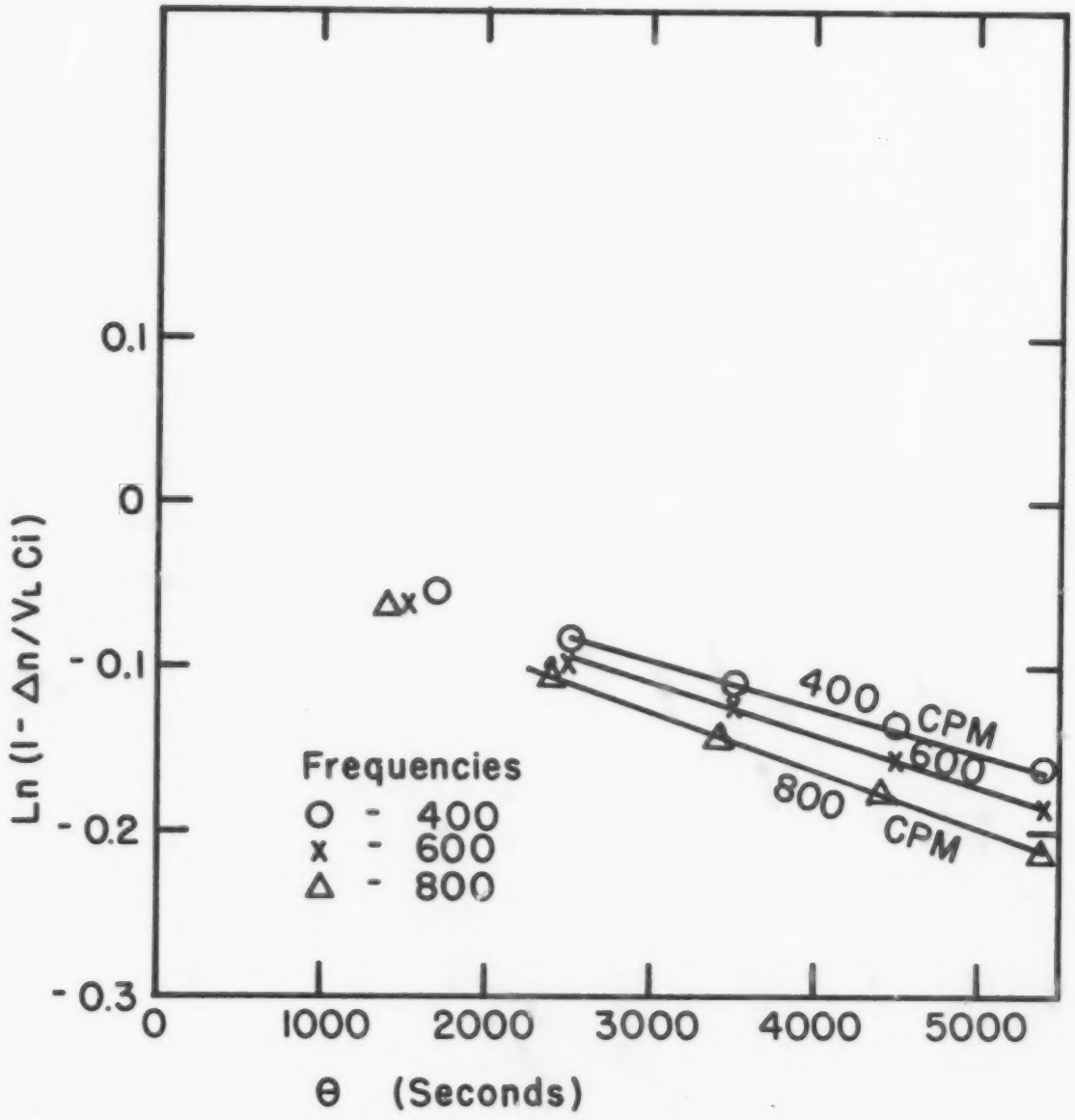

Figure 13. Propylene Absorption With Waves

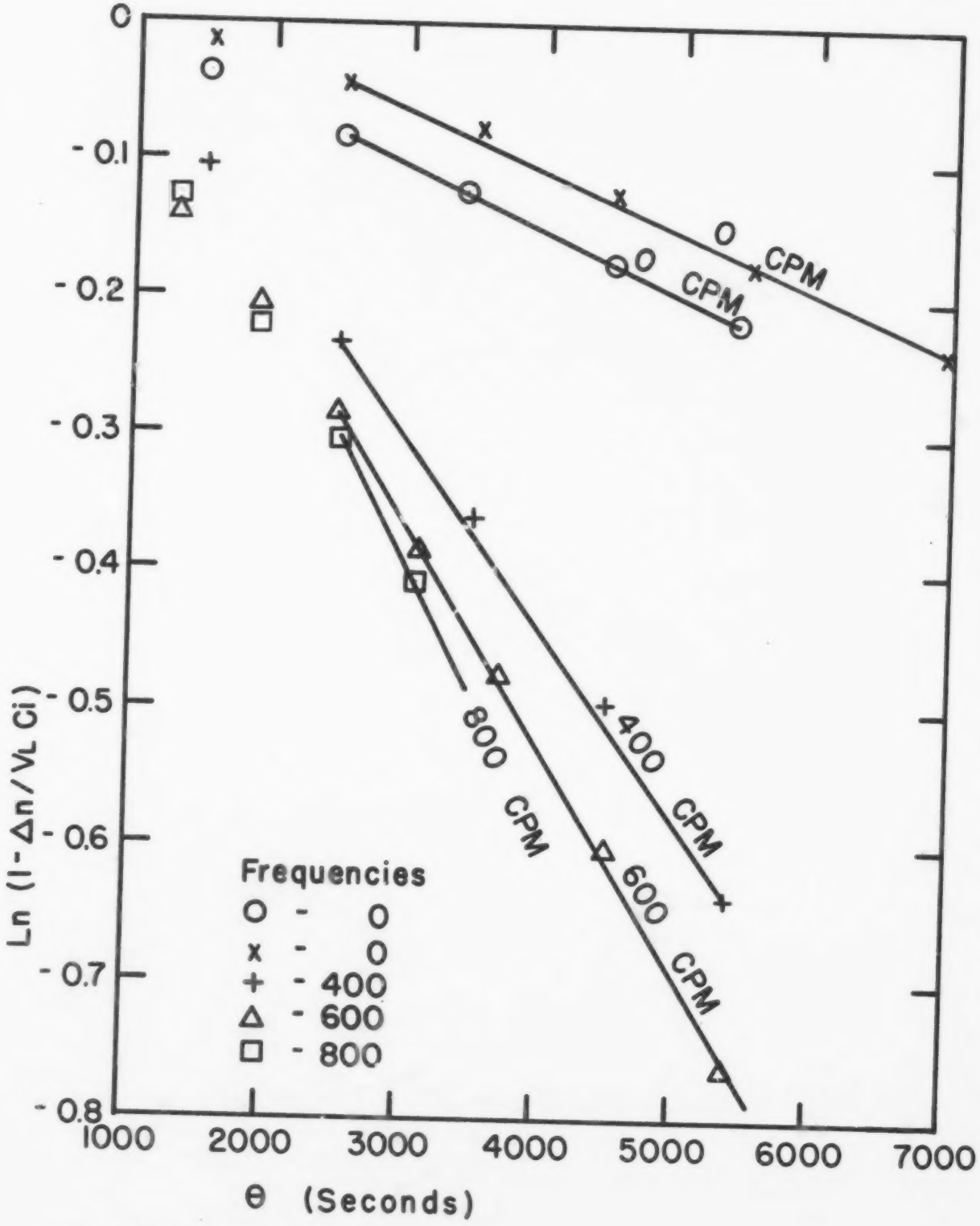

Figure 14. Helium Absorption

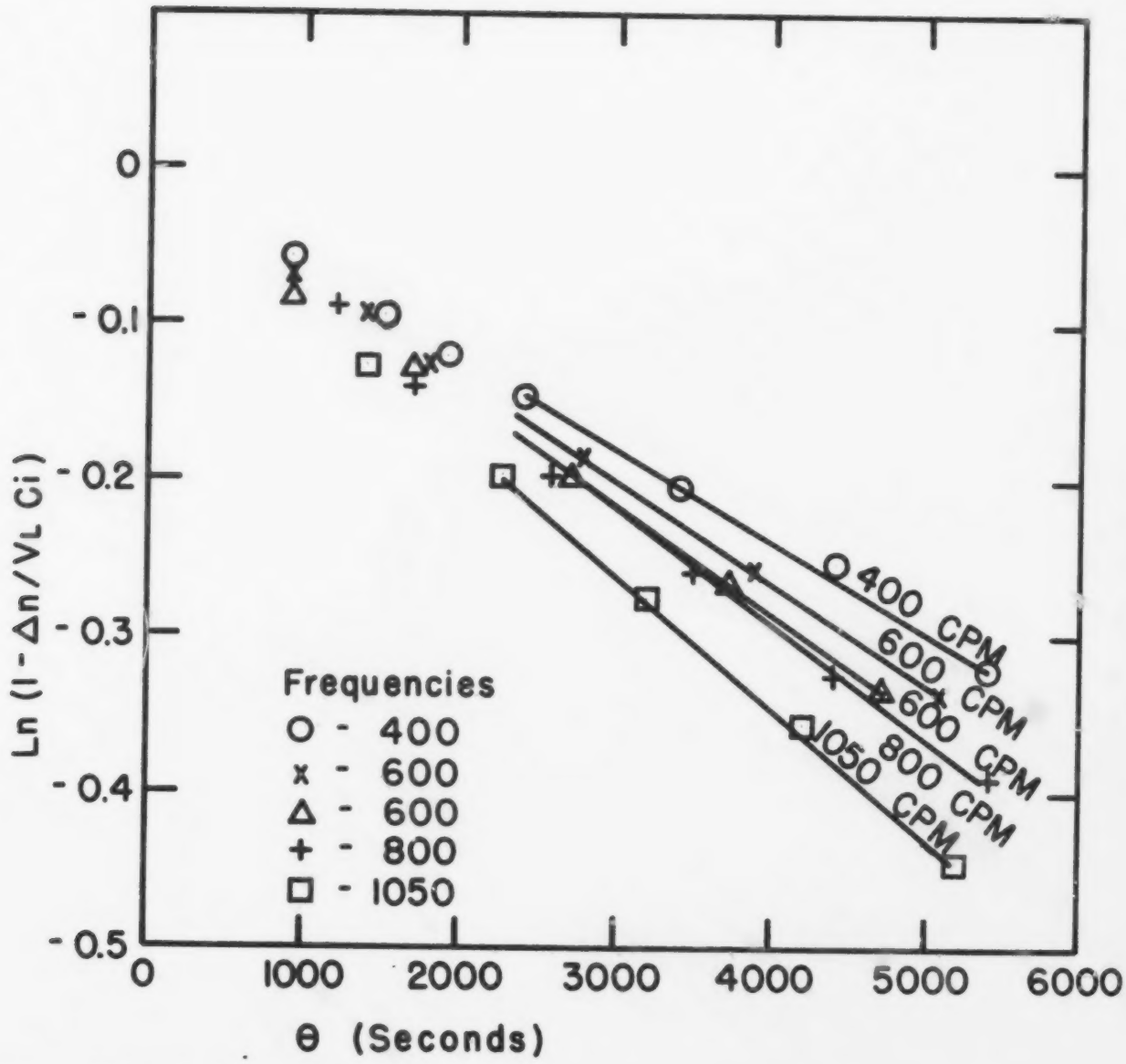

Figure 15. Carbon Dioxide Absorption With Waves

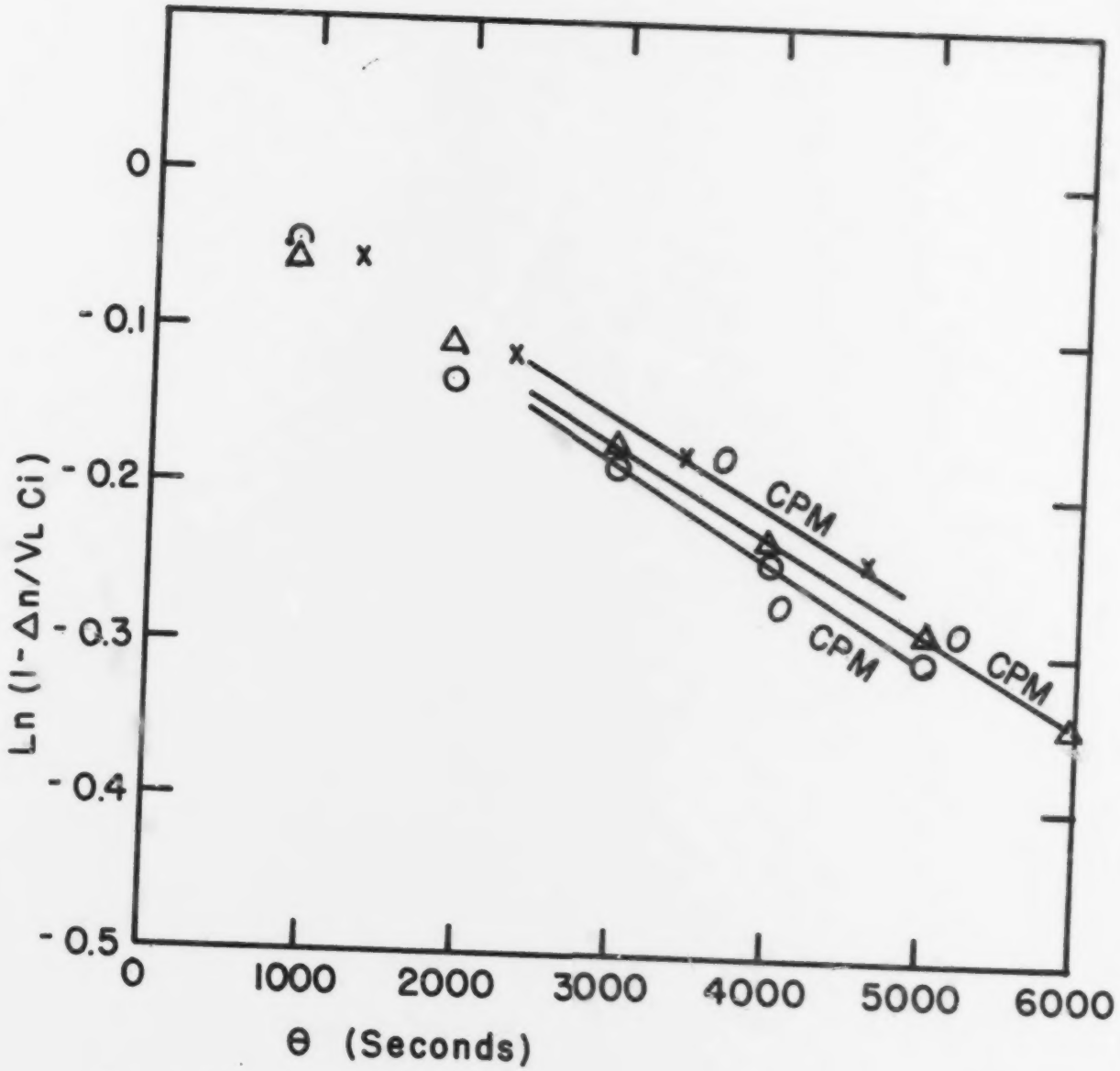

Figure 16. Carbon Dioxide Abscrption With No Waves

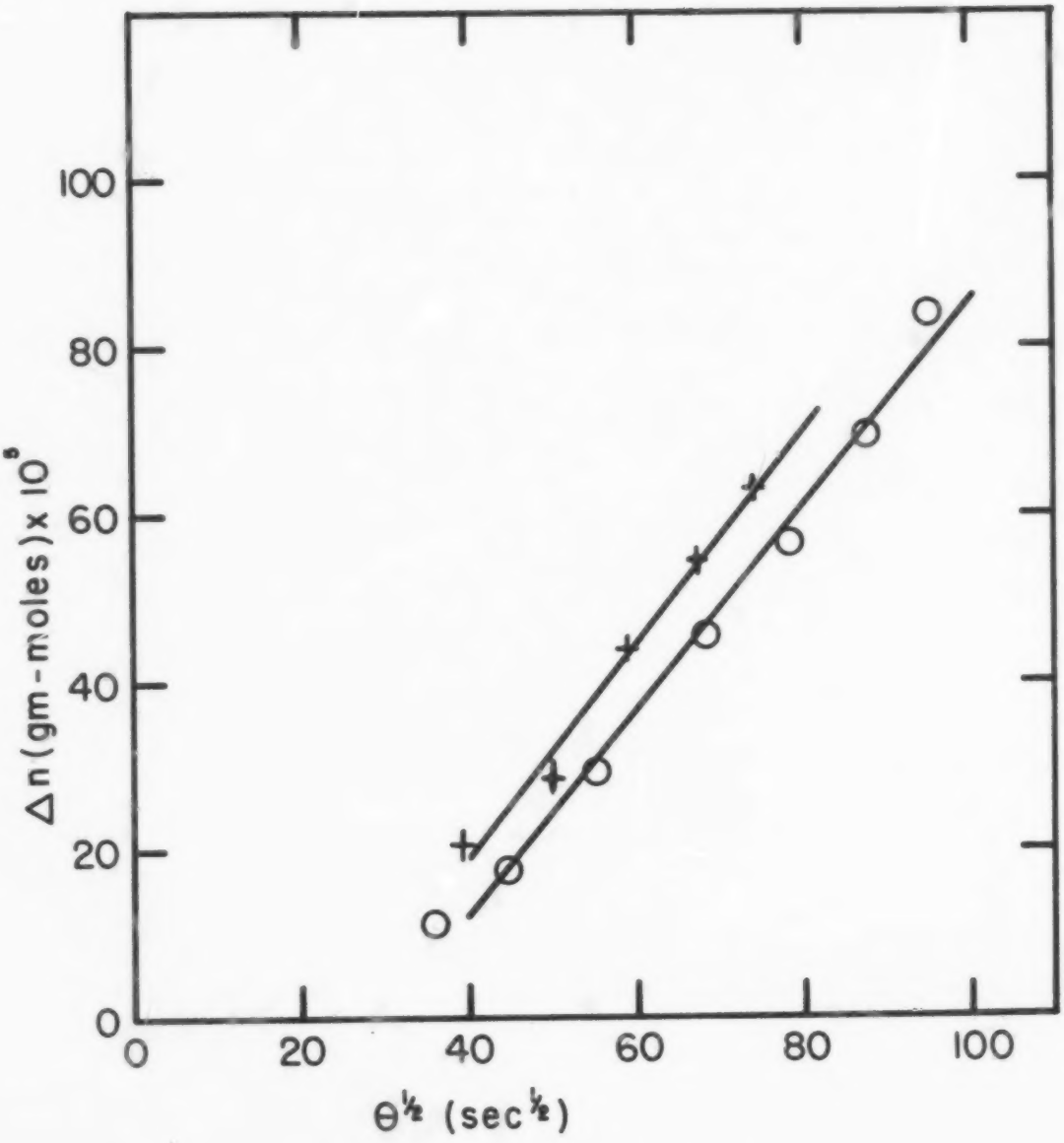

Figure 17. Oxygen Absorption With No Waves

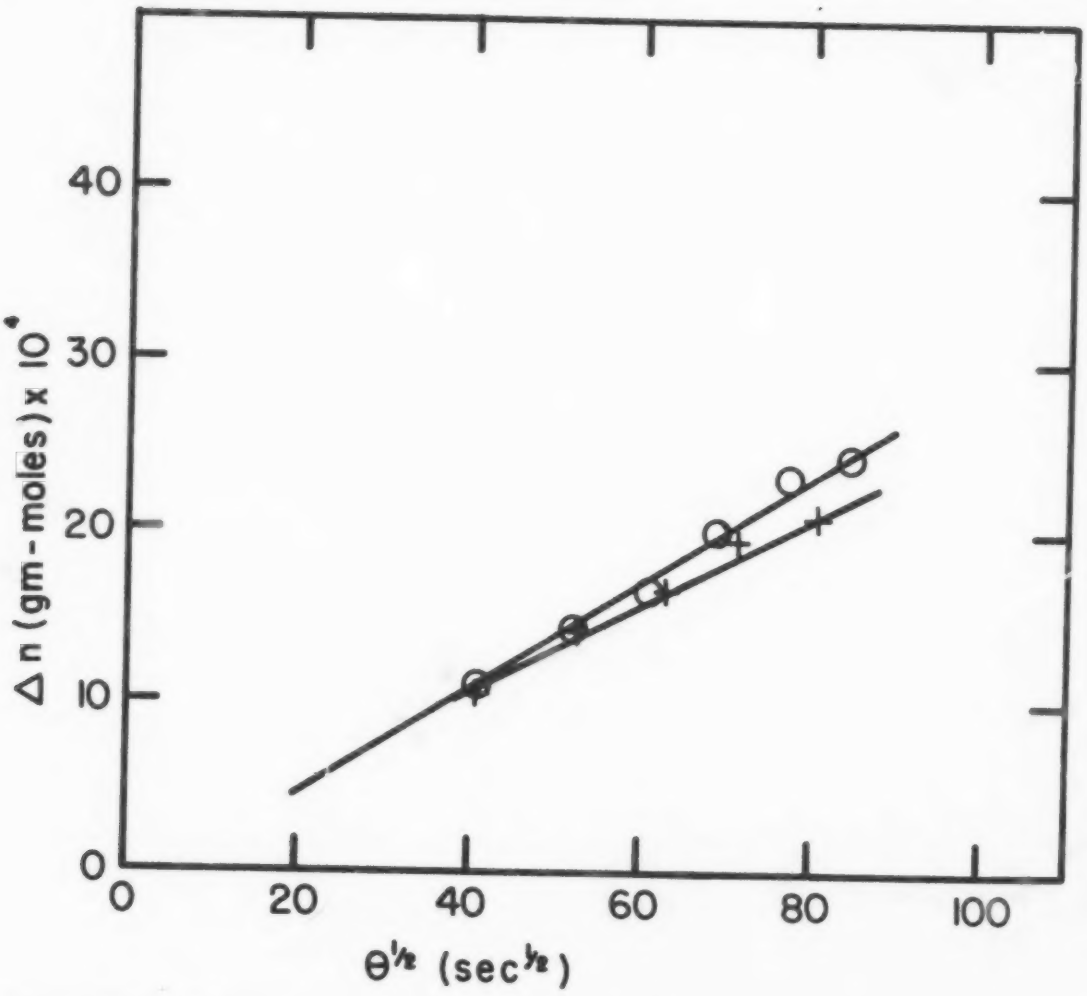

Figure 18. Propylene Absorption With No Waves

be plausible. This is illustrated by Figure 19, the data for Propylene. Such a conclusion, based on $d(\Delta n)/d\theta$ being constant (for times in excess of 900 seconds), could lead to a postulation of a psuedo steady state where

$$N = k(C_i - C_b) \quad . \tag{5-1}$$

k is a psuedo steady state mass transfer coefficient and C_i and C_b the interface and bulk concentrations respectively. The only apparent mechanism that could explain such behavior, is that of gross tank circulation due to secondary wave effects. It is conceivable that this circulation is such that fluid from the bulk continually comes to the surface, is enriched with solute there and then reenters the bulk. Thus, the surface can be pictured as the mass transfer analog to a heat exchanger. Consideration of inviscid and viscous second order wave theory (35) indicates that gross circulation currents, incorporating a film undergoing plug flow along the surface from the wave generator to the end of the tank, are possible.

This mechanism, however, shows definite contradiction. To begin with, the data indicate that the linear correlation of Δn vs. θ, if applicable, holds for the entire course of the run. The bulk concentration increases with time due to mass transfer, so that by a first approximation material balance

$$C_b = \Delta n \theta / V_L \quad . \tag{5-2}$$

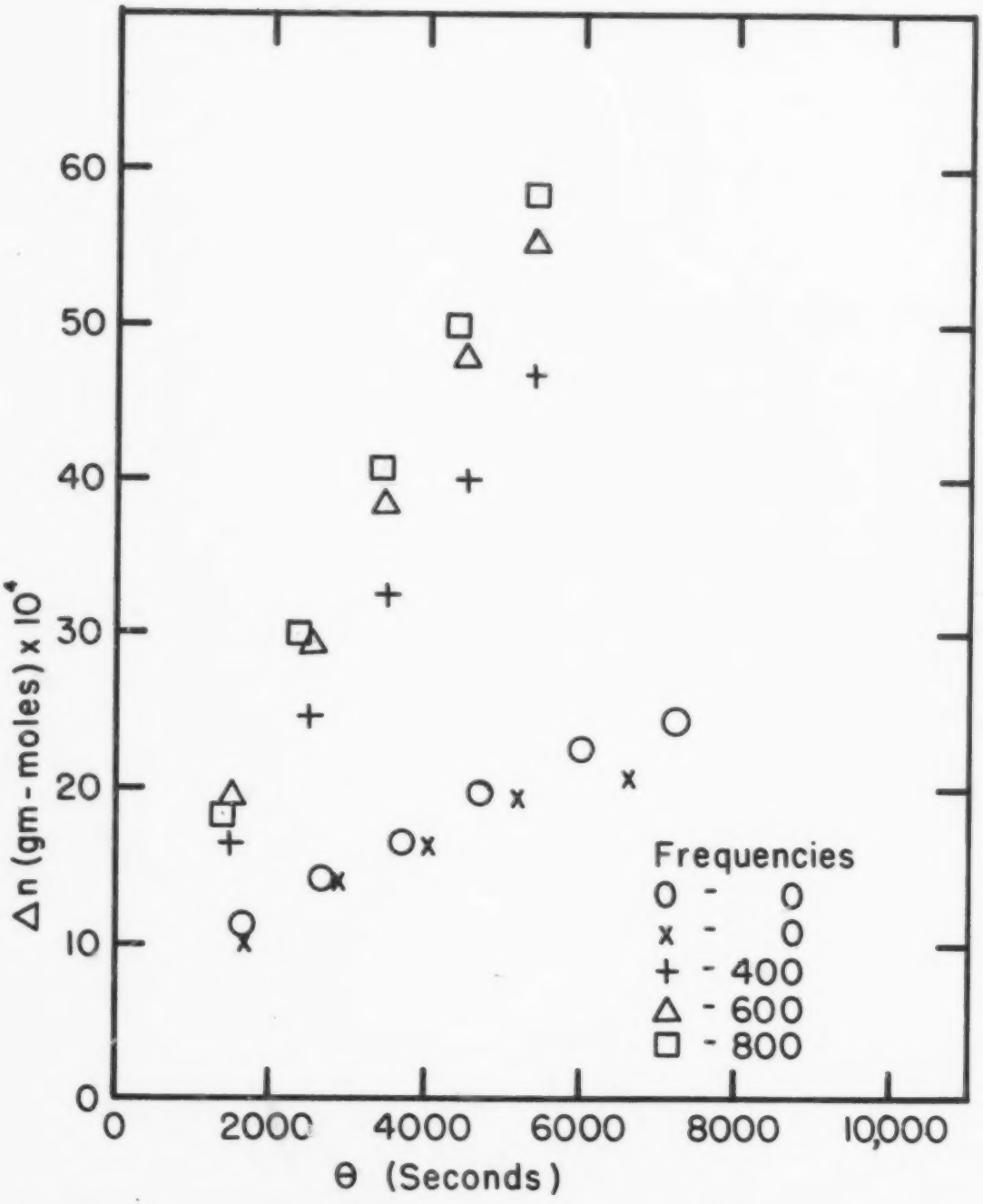

Figure 19. Experimental Propylene Absorption Data

Then

$$d\Delta n/d\theta = AN = Ak(C_i - \Delta n\theta/V_L) \qquad (5\text{-}3)$$

and this does not predict a constant $d\Delta n/d\theta$ with time. This is in contradiction to the experimental observations. The condition could only be realized for k increasing with time. The only plausible psuedo steady state mechanism, therefore, would be a circulation rate so slow, that for the course of a run only fresh water containing no solute comes to the surface. Then

$$d\Delta n/d\theta = Ak(C_i - 0) \qquad (5\text{-}4)$$

and values of k may be calculated from the slope. The implausibility of such k values is demonstrated by calculating them for 600 CPM runs for the four systems from least square fit straight line slopes. Making use of a film theory type correlation

$$k = D_w/\delta \quad , \qquad (5\text{-}5)$$

a film thickness δ , may be calculated. The results of these calculations shown in Table 5-1, indicate values of δ in the order of 1/2 to 2/3 of the liquid depth. Normally, the molecular diffusivity is used in (5-5) and this would make δ exceed this depth in nearly all the cases. This is quite contradictory to the physical mechanism as postulated and to the secondary drift velocity profiles predicted by hydrodynamic theory. The psuedo steady state mechanism is,

TABLE 5 - 1

PSUEDO STEADY STATE FILM THICKNESS

Frequency - 600 CPM

Gas	$D_W \times 10^4$ (cm^2/sec)	$k \times 10^5$ (cm/sec)	δ (cm)	δ/h
Helium	21.4	56.9	3.76	0.66
Oxygen	8.25	28.0	2.94	0.52
Carbon Dioxide	8.6	30.2	2.84	0.50
Propylene	4.1	15.8	2.60	0.46

therefore, discounted.

B. Comments on Effective Diffusivity

A qualitative appraisal of the values of D_w and D_w/D, immediately indicates an important feature. This is the fact that for none of the four gas systems do the no wave runs match predictions based on a molecular diffusion mechanism. This is illustrated by the D_w/D values for no wave runs. In all these cases the actual rate is higher than the molecular rate. The values of effective diffusivity, with the exception of Carbon Dioxide, vary in the order of increasing molecular diffusivity. D_w is greatest for Carbon Dioxide and the value (above 40) of D_w/D is well over that of the other systems.

As seen in Figure 20, the plot of D_w vs. frequency, the Propylene, Oxygen and Helium systems have D_w values in the proper order of their molecular diffusivities for a given frequency. Carbon Dioxide is out of order for all frequencies, but far less so in the driven runs than in no wave runs. Figure 20 shows that a smooth extrapolation of of driven values to the no wave value can only be made for Propylene. For Helium and Oxygen, extrapolation to zero frequency requires a sharp decrease in D_w. On the other hand, extrapolation for Carbon Dioxide requires an increase in D_w.

The above experimental observations lead to the conclusion that the liquid phase is not motionless during no wave

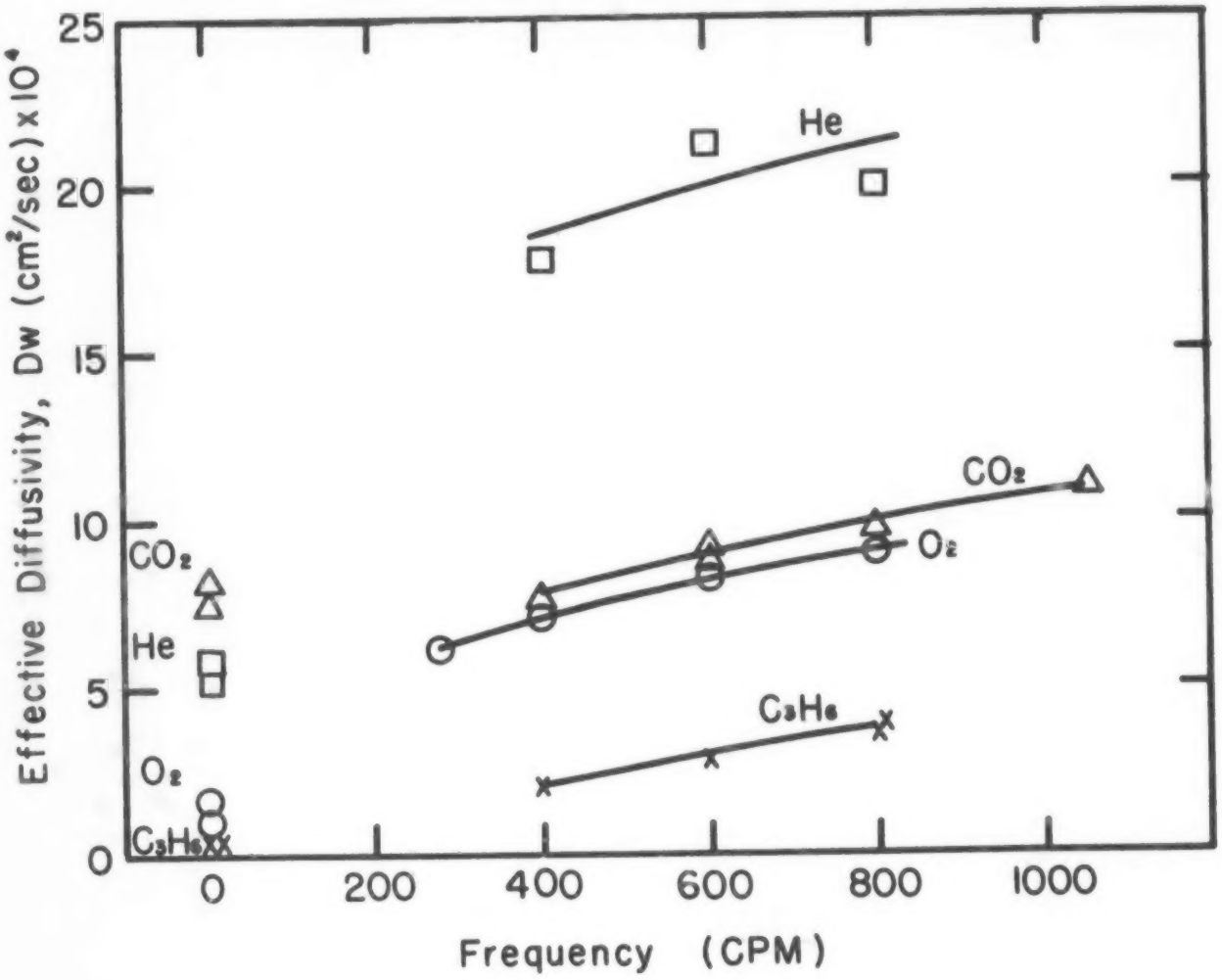

Figure 20. Effective Diffusivity for No Wave and Driven Runs

runs. The reproducibility of no wave D_w values, along with the different results for the various systems, indicates that motion is not due to random background vibrations. Rather, it is believed that natural convection currents, dependent on the properties of the system, are present. The change in relative position of Carbon Dioxide for wave as opposed to no wave runs, indicates that the mechanically imposed fluid motions tend to offset or dampen these currents. There does not appear to be a total domination by the forced motions, since Carbon Dioxide is still out of place with respect to molecular diffusivity in driven runs.

C. Discussion of No Wave Phenomena

Two mechanisms for natural convection exist. The first is the familiar bouyant effect, occurring when fluid density is changed due to mass or heat transfer. The most familiar case of this, occurs in fluids exposed to heated or cooled fixed surfaces (see e.g., McAdams (37)). In gas absorption there is a density change due to the act of solution as well as one due to the temperature effect of the heat of solution. Both could influence bouyant convection.

A second possible mechanism is due to surface motion arising from Marangoni Instability. This motion is caused by perturbations in surface concentrations, which in turn cause changes in surface tension and hence force imbalances. Associated with these surface motions are roll-cell motions in the body of the fluid. A detailed discussion of this

phenomenon is given by Sternling and Scriven (52). Its occurrence has primarily been observed at liquid-liquid interfaces. The magnitude of the effect in gas-liquid systems is unknown.

It must be noted that all four gases studied have a very low solubility in water. This is especially true for Oxygen and Helium. Thus, any change in liquid density or surface tension resulting from absorption would be expected to be very slight. Still, such effects appear to have a significant affect on mass transfer.

The Grashof Number is generally used to characterize the tendency for bouyant natural convection in a system (see e.g., Bird, Stewart and Lightfoot (6)).

$$Gr = g\rho^2 \gamma d^3 \Delta z/\mu^2 \qquad (5\text{-}6)$$

where g is the gravity constant, d a characteristic distance (taken as the tank depth, h, for this case) and Δz the change in solute concentration (mole fraction) causing natural convection. The quantity γ is given by

$$\gamma = (1/\rho)(d\rho/dz) \quad . \qquad (5\text{-}7)$$

Since there is both a concentration and temperature effect

$$d\rho/dz = (\partial\rho/\partial z)_T + (\partial\rho/\partial T)_z (dT/dz) \quad . \qquad (5\text{-}8)$$

Since

$$dT = (H_s/C_p)dz \quad , \qquad (5\text{-}9)$$

$$d\rho/dz = (\partial\rho/\partial z)_T + (H_s/C_p)(\partial\rho/\partial T)_z \qquad (5\text{-}10)$$

where an adiabatic heating effect is assumed. C_p is the specific heat of the solution, while H_s is the heat of solution for the system and is taken as positive when heat is generated by solution. H_s is known for Carbon Dioxide and can be estimated from equilibrium solubility data for the other systems by a Clausius-Clayperon relation. Since these are very dilute aqueous solutions $(\partial\rho/\partial T)_z$ can be obtained from density vs. temperature data for water. (e.g., (42)). Values for $(\partial\rho/\partial z)_T$ are not available, however. An estimation of this quantity can be obtained by assuming ideal saturated solutions and calculating density by use of additive partial volumes and linearizing the change; i.e.,

$$(\partial\rho/\partial z)_T = (\rho_s - \rho_w)/z_s \qquad (5\text{-}11)$$

where ρ_s and z_s are the saturation density and mole fraction respectively and ρ_w is the density of pure water. A value of liquid density for the solute component in its pure state is necessary for the ideal solution calculation. In order to estimate a Grashof Number for data correlation, saturated liquid densities were used for Carbon Dioxide and Propylene. Since the runs were made at temperatures well above the critical point for Oxygen and Helium, critical densities were used for these substances. Setting

$$\Delta z = z_s \qquad (5\text{-}12)$$

Grashof Numbers were calculated by (5-6) through (5-11).

These values are shown in Table 5-2.

In all cases, the calculations predict a decrease in density due to solution, so that negative values of Grashof Number result. This indicates a condition of bouyant stability, since the density gradient that is set up is in the same direction as the gravitational field for the physical situation at hand. This is analogous to exposing a heated surface facing downward, to a fluid. Experimenters have observed significant convection for this heat transfer case, in spite of inherent stability (37). These experiments, however, used heated plates of finite length and the fluid (gas) was free to flow upward around the sides of the plate. The experimental system for the situation herein discussed allows no analogous upward flow so that bouyant stability probably exists for systems where density decreases with solute concentration.

The Grashof Numbers of Table 5-2, are in doubt because of the inaccuracies of the calculation assumptions. Still they may reflect data trends. In correlating turbulent mass (and heat) transfer coefficients, the product of Grashof and Schmidt (or Prandtl) Number has been used (37). This product is not necessarily of similar value for an unsteady state "turbulent transport" effective diffusivity. Figure 21 is a plot of D_w/D vs. Gr. The data point for Carbon Dioxide does not correlate with the other systems. This system is dealt with further on in this section. Excluding Carbon Dioxide, Figure 21 indicates a drop of D_w/D with increasing Grashof

TABLE 5 - 2

GRASHOF NUMBER (Ideal Solution Assumption)

Gas	$Gr \times 10^{-4}$
Propylene	-114.5
Oxygen	- 11.05
Helium	- 3.55
Carbon Dioxide	-291

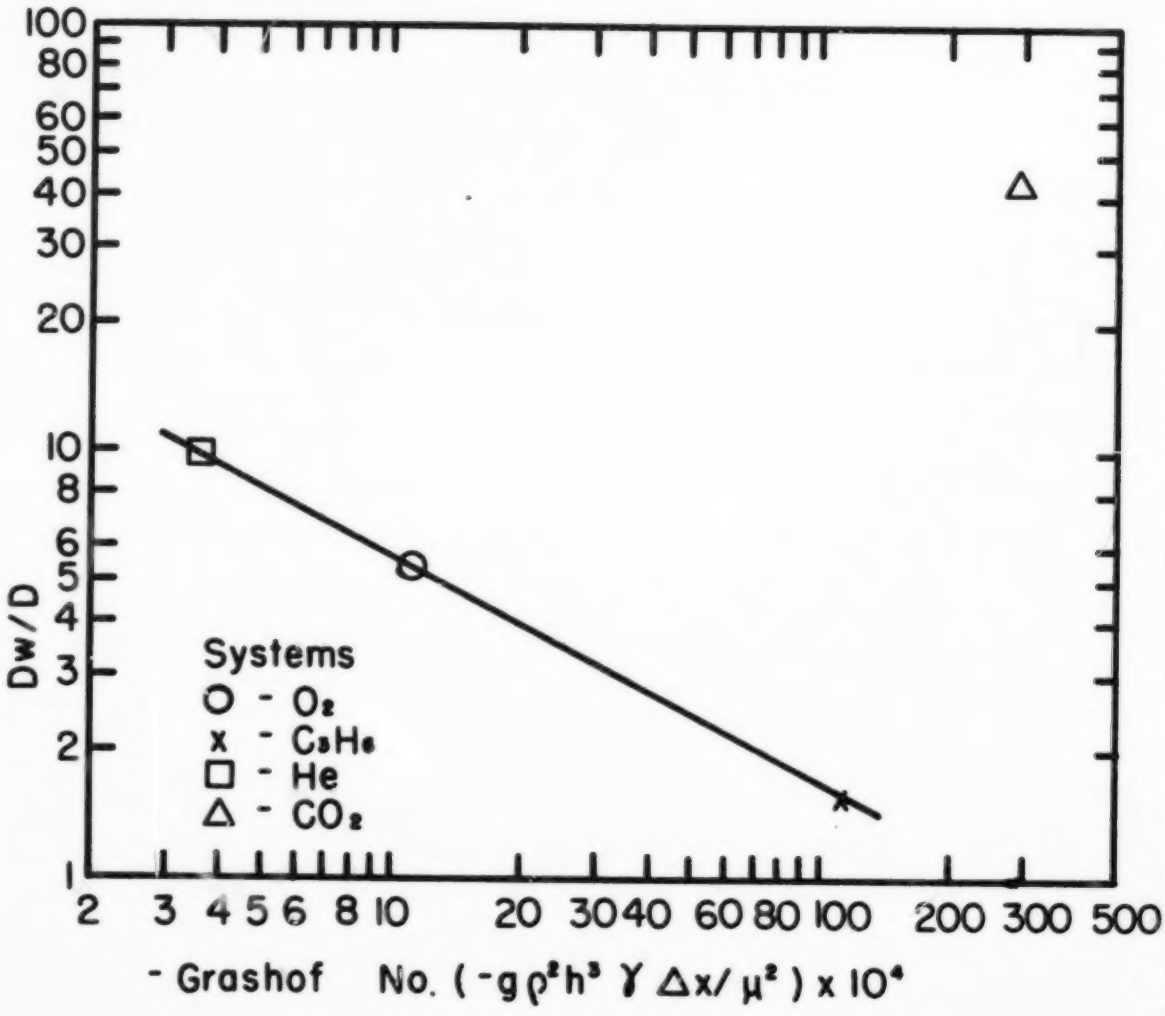

Figure 21. Role of Bouyant Forces in No Wave Case

magnitude (note negative Gr is plotted). This agrees with the bouyant stability concept and probably indicates that bouyant convection effects are not significant for Oxygen, Helium or Propylene.

Surface tension effects may, therefore, be the primary source of no wave motion for these systems. No data on the effect of solution on surface tension for these systems was found. Because of the small solubilities, it would be extremely difficult to measure this effect. An estimation based on theory is possible. The derivation described below is similar to that of Kuper and Trevena (29) and was suggested by that source.

For a pure liquid in equilibrium with its own vapor, surface tension may be expressed by the McLeod Equation.

$$\sigma^{1/4} = (\rho_L - \rho_V)(P/M) \qquad (5\text{-}13)$$

where ρ_L and ρ_V are the liquid and vapor phase densities respectively. P is the property known as the Parachor and M is the molecular weight. For a binary mixture this is written as

$$\sigma^{1/4} = \rho_L P_L/M_L - \rho_V P_V/M_V \qquad (5\text{-}14)$$

with distinct Parachor and molecular weight values for each phase. Since $\rho_V \ll \rho_L$ and the P and M values are of the same magnitude, the second term is neglected so that

$$\sigma^{1/4} = \rho_L P_L/M_L \quad . \qquad (5\text{-}15)$$

By the method of Fowler (29), the parachor may be expressed by

$$P = \omega a^{1/4} b^{7/12} \qquad (5\text{-}16)$$

where a and b are the van der Waal's constants for the substance being considered. ω is a constant related to Avogadro's Number. By the theory of Wall and Stent (29), for binary mixtures

$$a = z_1^2 a_1 + 2z_1 z_2 a_{12} + z_2^2 a_2 \qquad (5\text{-}17)$$

$$b = z_1 b_1 + z_2 b_2 \qquad (5\text{-}18)$$

where z is mole fraction and the subscripts refer to the 2 components. a_{12} is an interaction constant and can be estimated as $(a_1 a_2)^{1/2}$. Let $z = z_1$ be the mole fraction of the solute so that $z_2 = (1 - z)$. Making this substitution, note that z^2 is extremely small and can be neglected due to the small solubilities of the systems of this dissertation. Then

$$a = a_w + 2z((a_v a_w)^{1/2} - a_w) \qquad (5\text{-}19)$$

$$b = b_w + z(b_v - b_w) \quad . \qquad (5\text{-}20)$$

Note the subscripts 1 and 2 have been replaced by w (water) and v (vapor) respectively. Thus, for the liquid phase

$$P_L = (a_w + 2z((a_v a_w)^{1/2} - a_w))^{1/4} (b_w + z(b_v - b_w))^{7/12} \quad . \qquad (5\text{-}21)$$

Letting

$$K = \omega \rho_L / M_L \quad , \tag{5-22}$$

$$\sigma = K^4 (a_w + 2z((a_v a_w)^{1/2} - a_w))(b_w + z(b_v - b_w))^{7/3} \quad . \tag{5-23}$$

To estimate the change of surface tension with concentration, differentiate and get

$$\partial \sigma / \partial z = 2K^4((a_w a_v)^{1/2} - a_w)(b_w + z(b_v - b_w))^{7/3} + (7/3)K^4(a_w + 2z((a_w a_v)^{1/2} - a_w))(b_w + z(b_v - b_w))^{4/3}(b_v - b_w). \tag{5-24}$$

Since z, the solute concentration, is small the terms with z coefficients are neglected. Then

$$\partial \sigma / \partial z = 2K^4 b_w^{7/3}((a_v a_w)^{1/2} - a_w) + (7/3)K^4 a_w b_w^{4/3}(b_v - b_w) \quad . \tag{5-25}$$

By equation (5-15) and (5-16) for water

$$\sigma = K^4 a_w b_w^{7/3} \tag{5-26}$$

where it is assumed that the density and molecular weight of the solution are equal to that of water (very dilute solutions). Thus, using σ for water as that of the solution

$$(1/\sigma)(\partial \sigma / \partial z) = 2((a_v/a_w)^{1/2} - 1) + (7/3)(b_v/b_w - 1) \quad . \tag{5-27}$$

The applicability of the dimensionless group $(1/\sigma)(\partial \sigma / \partial z)$ is now discussed. Qualitatively, this should be a measure of the degree of force imbalance resulting from a surface concentration perturbation. (Marangoni Instability) This is supported by examining one of the equations governing surface tension instability as set forth by Sternling and Scriven (52) and later by Scriven (49).

$$\partial \sigma_{yy}/\partial y=(d\sigma/dC_i)(\partial C_i/\partial y)+\mu_s(\partial^2 v/\partial y^2) \qquad (5\text{-}28)$$

at the surface. Here σ_{yy} is the "y component of longitudinal surface stress" with the same units as surface tension and μ_s is the "composite surface viscosity" with units of mass/time. (See Sternling and Scriven (52).) (5-28) is modified by the definition of various dimensionless quantities as follows:

$$\sigma^*_{yy} = \sigma_{yy}/\sigma \quad \text{(dimensionless stress)} \qquad (5\text{-}29)$$

$$y^* = y/L \quad \text{(dimensionless distance)} \qquad 5\text{-}30)$$

$$v^* = vL\rho/\mu \quad \text{(dimensionless velocity)} \qquad (5\text{-}31)$$

Let

$$\Gamma = d\sigma/dC_i \qquad (5\text{-}32)$$

$$C^* = C/\rho_m \qquad (5\text{-}33)$$

where L is a characteristic system dimension not here defined. ρ_m is the molar density and for these dilute cases equilibrium mole fraction can be taken equal to C_i/ρ_m. Substituting (5-29) through (5-33) into equation (5-28) and rearranging gives the dimensionless equation

$$\partial \sigma^*_{yy}/\partial y^*+(\Gamma \rho_m/\sigma)(\partial C^*/\partial y^*)+(\mu_s \mu/L^2\rho\sigma)(\partial^2 v^*/\partial y^{*2}). \qquad (5\text{-}34)$$

This supports the possibility of using $(\Gamma \rho_m/\sigma)$ as a correlating dimensionless group. Note that

$$\Gamma \rho_m/\sigma = (1/\sigma)(\partial\sigma/\partial(C_i/\rho_m))=(1/\sigma)(\partial\sigma/\partial z)=N_\sigma \qquad (5\text{-}35)$$

which can be calculated by (5-27). Considering μ_s to be

equivalent to μL (note equality of dimensions) the other dimensionless coefficient becomes $\mu^2/L\rho\sigma$. This is the square of the Ohnesorge Number (see Perry (43)), which is used in atomization correlations. This number does not vary among the systems studied and is not considered further.

Values of N_σ along with equivalent values of D_w/D for no wave runs are presented in Table 5-3. Negative N_σ indicates a decrease of surface tension as concentration increases, with the reverse effect for a positve value. Since the surface tension effect is assumed to be initiated by random surface concentration perturbations, it would be expected that only the absolute value of N_σ should be of interest. However, the relatively high positive value for Propylene is difficult to accept. Strong bonding with water would not be expected for this compound so that dissolved Propylene would be expected to decrease surface tension. This discrepancy may be due to Propylene's normal boiling point being relatively close to the experimental temperature. Thus, van der Waal's Equation and constants may be least dependable for this gas. The change of D_w/D is consistent with N_σ for Oxygen and Helium. It is difficult to match values for Carbon Dioxide, if in fact bouyant effects dominate for that system. This is discussed further on in this section. Finally, it is important to note that by (5-27) the van der Waal constants for water (which is at ambient temperature and pressure) are incorporated in N_σ calculations for all the systems. Since water is a liquid under the experimental conditions, the

TABLE 5 - 3

SURFACE TENSION NUMBER

Gas	D_w/D	N_σ	$(N_\sigma \times Gr) \times 10^{-4}$
Propylene	1.77	4.46	-520
Oxygen	5.34	-0.415	4.6
Helium	9.85	-2.35	8.3
Carbon Dioxide	44.3	0.55	-161

applicability of van der Waal's Equation and hence the N_σ values are questionable.

For completeness an attempt to combine the available correlations for bouyant and surface tension effects is presented. The product of N_σ and Grashof Number (as previously calculated) is obtained and also presented in Table 5-3. No trend with D_w/D is observed. Again the question of the significance of a negative Grashof Number (predicting bouyant stability) must be brought up. However, excluding Propylene, there is a trend between the absolute value of the dimensionless product and D_w/D.

For an order of magnitude estimation of the relative effects of bouyancy and surface tension instability, consider the equation of motion for free convection as presented in the text of Bird, Stewart and Lightfoot (7).

$$(\rho)(D\bar{v}/D\theta) = \mu\nabla^2\bar{v} - \rho\gamma\bar{g}\Delta z \quad . \qquad (5\text{-}36)$$

From a consideration of the last term, the quantity $g\rho h\gamma\Delta z$ represents the energy available for bouyant motion where h is the liquid depth. By analogy, for surface tension $g\rho(1/\sigma)(\partial\sigma/\partial z)\Delta zW$ is the maximum energy for surface tension induced motion. In this expression, Δz represents the maximum surface concentration perturbation (saturated-pure water) possible and W is a surface length dimension, here taken as the width of the tank. Let ψ_s be the ratio of surface tension to bouyant energy.

$$\psi_s = (g\rho(1/\sigma)(\partial\sigma/\partial z)\Delta z W)/g\rho h r \Delta z = WN_\sigma / h r. \qquad (5\text{-}37)$$

ψ_s was calculated from the values of r, used to calculate the ideal solution values of Grashof Number and the N_σ values of Table 5-3. ψ_s values are tabulated in Table 5-4. Though the direction of the bouyant effect may be toward stability, r still is a measure of the order of magnitude of bouyant energy that could result from slightly soluble gas dissolving under conditions favorable to bouyant motions. The values of ψ_s do indicate significant surface tension effects.

Bouyant forces apparently act in the direction of stability and against the promotion of free convection in at least three of the four cases. Under this condition the bouyant forces should retard the rate of transfer. Therefore, surface tension effects are probably more important than the ψ_s values indicate.

In the case of Carbon Dioxide, the large value of D_w/D for no wave runs can only be explained by bouyant effects. Though there is no experimental evidence, it is conceivable that an ideal solution assumption is grossly in error for this system and that the solution of this gas causes an increase in density. This statement has been made by Danckwerts (19), though he cites no reference. Under such a condition a state of bouyant instability results, being analogous to fluid contacting a heated plate facing upward. Also the relatively high (compared to the other systems studied) solubility of Carbon Dioxide in water, is manifested in the high D_w/D value,

TABLE 5 - 4

VALUES OF ψ_s, EQUATION (5-37)

Gas	ψ_s
Propylene	-5.45
Oxygen	0.66
Helium	28.9
Carbon Dioxide	-0.64

by this increase of density mechanism.

One other consideration for the Carbon Dioxide system is the effect of its reaction with water to form Carbonic Acid. This is not believed to be influential since ionization constant data indicates a very low concentration of carbonate and bicarbonate ions compared to molecular Carbon Dioxide. Furthermore, these ions would be expected to have diffusivity values close to that of Carbon Dioxide and the effect on concentration gradient should be minimal.

D. Wave Effects

Experimental results clearly indicate an increase of D_w with frequency for the driven runs of all four systems. A correlation of dimensionless groups, indicating this relation is desired. Such a correlation is realized by defining the group

$$F = fh^2/D \qquad (-38)$$

where f is the wave frequency. The relating equation is of the form

$$D_w/D = K_1 F^{\alpha} \quad . \qquad (5-39)$$

Values of F are included in Table A-8. Figure 22 is a log-log plot of D_w/D vs. F for all systems. A slope of 1/3 (see solid lines of Figure 22) yields a good fit to the data of the four cases and thus α is determined as 1/3. Values of K_1, determined by the intercepts of the lines are listed in Table 5-5.

TABLE 5 - 5

VALUES OF K_1, EQUATION (5-39)

Gas	K_1
Oxygen	0.15
Propylene	0.098
Helium	0.204
Carbon Dioxide	0.182

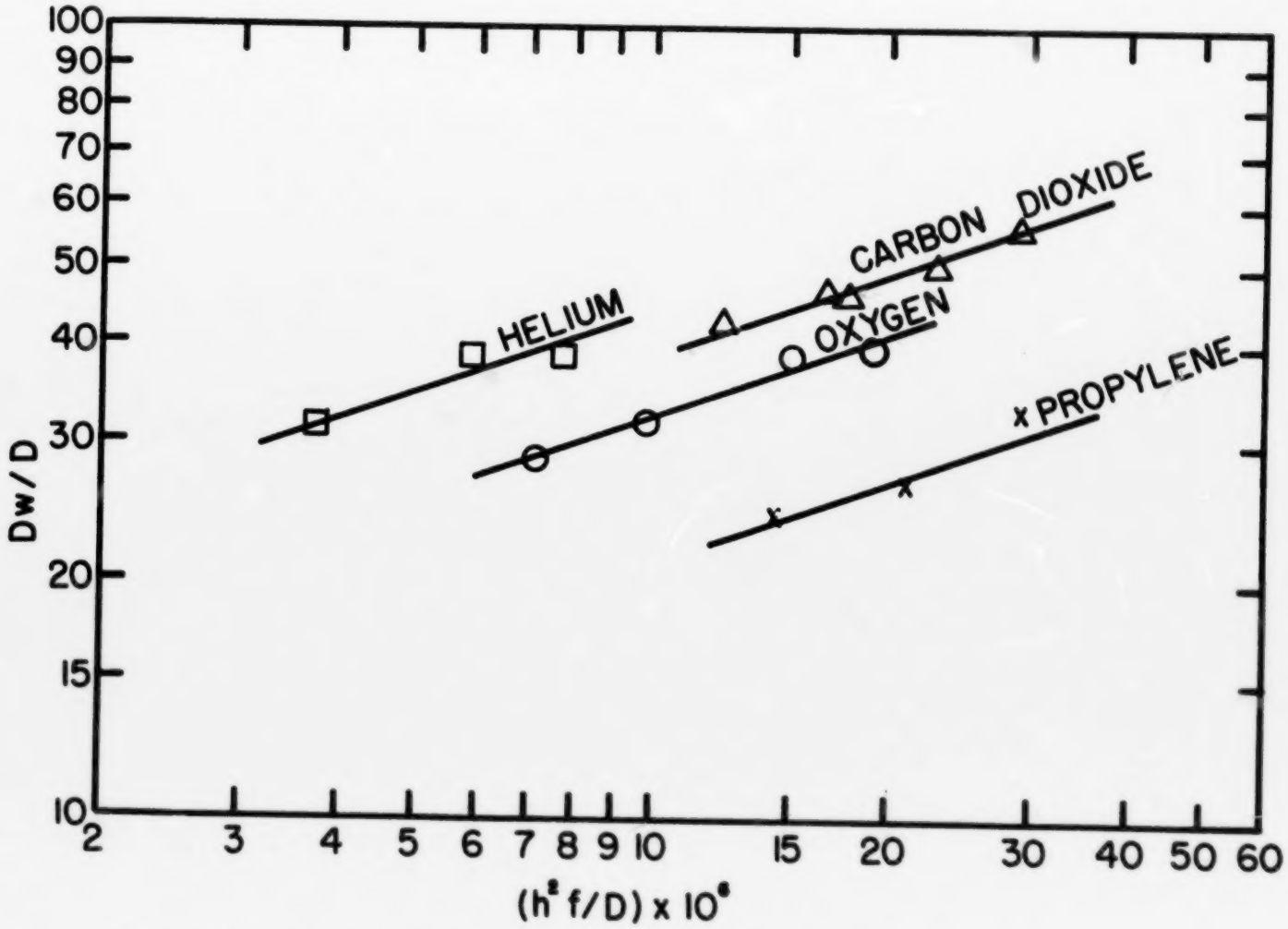

Figure 22. Influence of Frequency on Effective Diffusivity

Examination of Figure 22, shows that at any given value of F, the D_w/D value for Carbon Dioxide is out of place with respect to molecular diffusivity. This again reflects the fact that some degree of natural convection is present in driven runs for this system and can be further illustrated by considering the equations of motion for forced and free convection as presented by Bird, Stewart and Lightfoot (7).

$$(\rho)(Dv/D\theta) = \mu \nabla^2 v + \begin{cases} -\nabla p + \rho g & \text{(forced} \\ -\rho r g \Delta z & \text{(free)} \end{cases} \qquad (5\text{-}40)$$

A rough order of magnitude comparison between net wave potential energy (due to fluid height fluctuation) and bouyant energy, is obtained by comparing $g\rho a$ and $g\rho h r \Delta z$, where r and Δz are as defined for the definition of Grashof Number and a is the wave amplitude. The ∇p term of (5-40) is neglected since variation of static pressure at the free surface is considered to be negligible. Define the ratio ψ by

$$\psi = |g\rho h r \Delta z| / |g\rho a| = |h r \Delta z / a| \quad . \qquad (5\text{-}41)$$

Using Δz corresponding to saturation, the ideal solution values of r and the average amplitude (as determined by the experiments of Chapter III), ψ is calculated at 600 CPM for the four systems. The results are presented in Table 5-6. ψ is a ratio of bouyant to wave energy and for Carbon Dioxide it is seen that these energies are in the same order of magnitude.

Returning to (5-39), if Carbon Dioxide is excluded the

TABLE 5 - 6

VALUES OF ψ, EQUATION (5-41)

Frequency - 600 CPM

Gas	ψ
Helium	0.0027
Oxygen	0.0083
Carbon Dioxide	0.202
Propylene	0.0805

values of K_1 are in order of molecular diffusivities. This suggests a relationship of the form

$$D_w/D = K_2(Sc)^{\beta} F^{1/3} \qquad (5\text{-}42)$$

where Sc (the Schmidt Number is the ratio $\mu/\rho D$. Figure 23 is a plot of $(D_w/D)F^{1/3}$ vs. Sc for Oxygen, Helium and Propylene. The slope and intercept, determined by the method of least squares (solid line) give values for β and K_2. (5-42) then becomes

$$D_w/D = 2.74\ (Sc)^{-1/2} F^{1/3} \qquad (5\text{-}43)$$

where the value of β actually was -0.508 but was rounded off to -1/2. Realizing that

$$F = fh^2/D = (Sc)(fh^2\rho/\mu) \quad , \qquad (5\text{-}44)$$

(5-43) may be rewritten as

$$D_w/D = 2.74\ (\mu/\rho D)^{-1/6}(fh^2\rho/\mu)^{1/3} \quad . \qquad (5\text{-}45)$$

The group $(fh^2\rho/\mu)$ may be thought of as a wave Reynolds Number.

E. General Remarks

Before concluding this chapter, two other subjects deserve comment. The first is the effect on mass transfer of the increase in surface area due to waves. This change is negligible for the physical experiments previously described. Amplitude to wave length ratios were on the average below

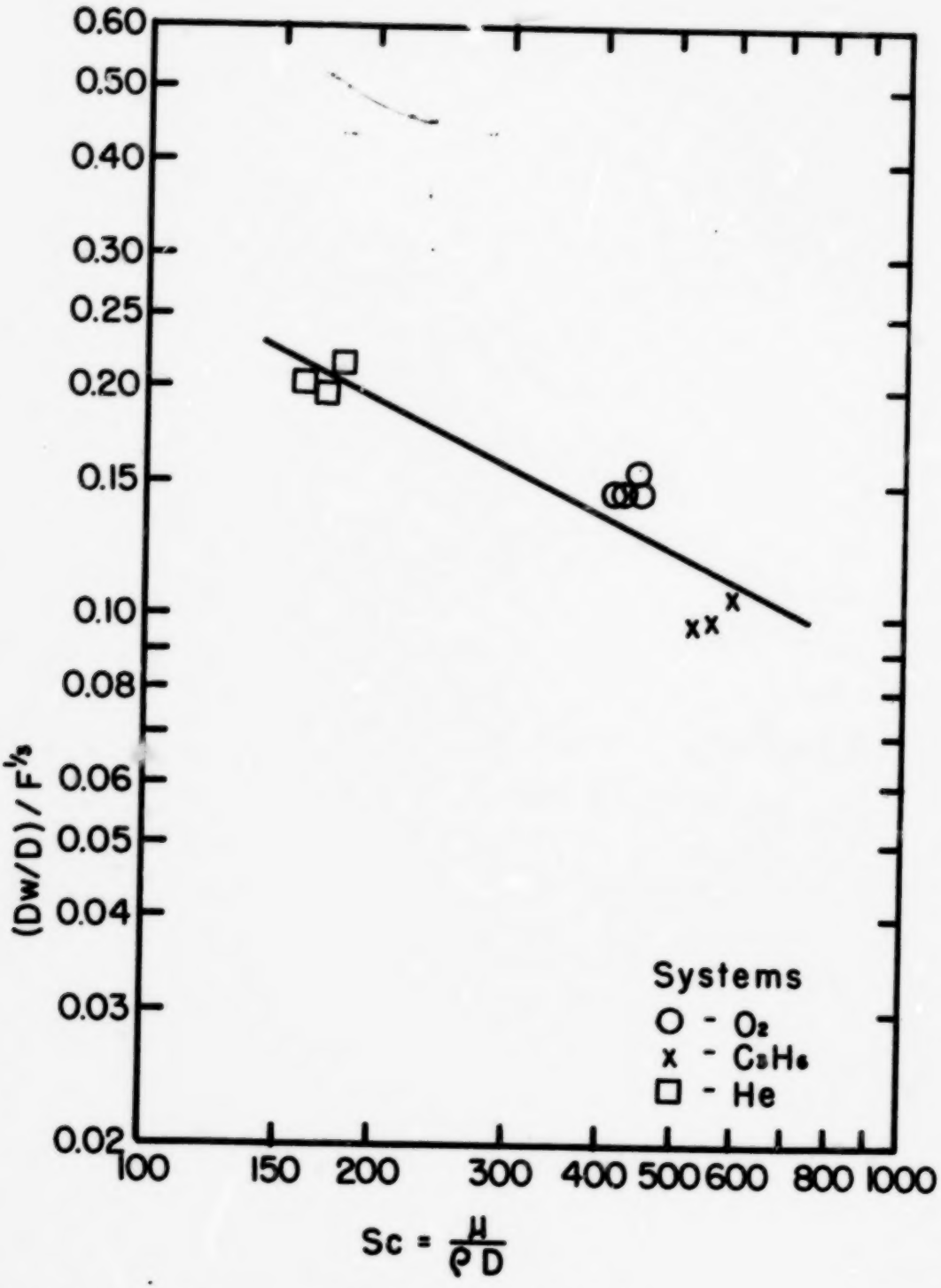

Figure 23. Effect of Molecular Diffusivity

0.05. Surface area must be kept in mind, however, when working with waves of higher amplitude.

The second subject is that of turbulence. The possibility of turbulent variations to smooth particle paths was discussed in Chapter II. Such perturbations would be expected to occur in all three dimensions and surface motions in the width direction (3rd dimension) would be expected. Since such motions were not observed over the experimental frequency range, it is concluded that little flow turbulence was present. It would be helpful to establish a Reynolds Number criteria for the inception of turbulence, but the arbitrariness of the choice of characteristic distance makes this difficult.

In the absence of turbulence, smooth particle paths, wherein neighboring particles move with only very small changes in relative position, are indicated. This would point to second order drift motions as the major mechanism of increase of mass transfer with increasing frequency. First order wave motions, however, apparently damp out natural convection motions.

CHAPTER VI

CONCLUSIONS

Diffusion is a relatively slow process. For this reason, practical applications make use of increased surface area resulting from the dispersion of one of the fluids as droplets, bubbles or thin films. Equipment is such that perturbation induced waves probably occur at numerous locations. Therefore, there is little motivation to design mechanical wave generation devices for promoting mass transfer. However, the periodic motion at and near the interface should be considered in fundamental analysis of existing methods. To this end the results of this study provide worthwhile information.

Direct experimental analysis indicates that effective diffusivity for wave situations is as much as twenty times the effective diffusivity for the corresponding no wave case. This largest value was for Propylene at 800 CPM. The ratio was considerably smaller for Oxygen, Helium and Propylene. In all cases the mass transfer rate tended to level off with increasing frequency, so that frequencies higher than those measured would not be expected to significantly increase rate.

Summarizing the discussion of Chapter V, the increase in

in mass transfer over that predicted by molecular diffusion for no wave runs, is attributed to natural convection motions. For the Oxygen, Helium and Propylene systems, the governing mechanism appears to be instability caused by surface tension inbalances due to surface concentration perturbations, (Marangoni Effect). In the case of Carbon Dioxide, bouyant instability caused by density increase due to solution may be the more significant mechanism. Both these phenomena are worthy of further experimental investigation since they are of fundamental importance to fluid mass transfer. It is significant that they are manifested in systems of as low a solubility level as those explored in this dissertation.

The effects of surface waves lead to the conclusion that mechanically forced motion tends to damp out or offset natural convection. Thus, the mechanism relating mass transfer to wave activity lies in the particle motions due to the waves. First order closed path flows, by their nature can contribute little toward increasing concentration gradient. It is concluded that second order particle migrations are primarily responsible for wave effects on mass transfer. A worthwhile scheme for further experimentation, would be to aim for hydrodynamic conditions (e.g., lower frequencies) where drift migrations are minimized and thus the effects of first order motions alone. From a hydrodynamic standpoint it would be of interest to explore the effect on transfer of varying liquid depth. The dimensionless quantities, incorporating frequency, of Chapter V (fh^2/D and $fh^2\rho/\mu$), may be useful in correlating

the effect of waves and oscillations in future experiments and in other mass transfer situations.

The experimental methods described in this dissertation, were for the most part, original in nature and should be useful in similar experiments. The optical method for determining wave amplitude may be used as a means of viewing waved surfaces and could be used to observe the onset of hydrodynamic instability at the surface.

Because of the lack of adequate data or means of measuring density and surface tension changes with concentration, as well as the limitations on hydrodynamic theory due to viscous effects, the analysis has been qualitative at many points. It has, however, raised questions regarding the basic nature of absorption and more generally, mass transfer. Though clear cut answers are not always available, directions for further exploration have been defined and significant experimental facts established. This along with the useful experimental techniques, is the major contribution of this dissertation.

APPENDIX A

LISTING OF DATA AND TABULATED QUANTITIES

Table A-1 Through A-8

TABLE A - 1

AMPLITUDE DATA

A. Frequency - 400 CPM

Tank Position (cm)	Screen Height (cm)	S	Amplitude (cm)
13.8	32.0	0.059	0.0585
13.1	27.6	0.0145	0.061
13.5	30.0	0.015	0.063
12.8	30.0	0.015	0.063
6.9	12.7	0.036	0.151
8.6	12.7	0.0342	0.144
8.7	11.4	0.034	0.143
21.0	28.3	0.0134	0.056
21.5	26.7	0.015	0.063
20.5	28.3	0.0123	0.0515

B. Frequency - 500 CPM

Tank Position (cm)	Screen Height (cm)	S	Amplitude (cm)
14.5	32.0	0.0836	0.028
12.4	27.6	0.125	0.03
13.4	27.6	0.070	0.033
13.4	30.0	0.115	0.0276
7.8	12.7	0.0796	0.0715
7.2	12.7	0.0796	0.0715
8.4	11.4	0.128	0.070
19.6	35.8	0.143	0.0216
20.7	38.0	0.086	0.0235

C. Frequency - 600 CPM

Tank Position (cm)	Screen Height (cm)	S	Amplitude (cm)
13.6	32.0	0.107	0.016
14.4	27.6	0.0715	0.0205
13.2	30.0	0.146	0.016
15.4	30.0	0.128	0.0164
7.5	12.7	0.061	0.046
7.9	11.4	0.142	0.0415
20.3	34.2	0.165	0.0124

TABLE A - 1 (Continued)

D. Frequency - 700 CPM

Tank Position (cm)	Screen Height (cm)	S	Amplitude (cm)
15.2	27.6	0.084	0.0126
14.2	27.6	0.084	0.0126
13.5	30.0	0.174	0.0102
14.7	30.0	0.174	0.0102
8.2	12.7	0.121	0.028
6.2	12.7	0.097	0.0296
7.2	11.4	0.145	0.0293
19.1	36.0	0.109	0.0102
22.0	36.0	0.109	0.0102

E. Frequency - 800 CPM

Tank Position (cm)	Screen Height (cm)	S	Amplitude (cm)
12.1	22.2	0.123	0.0124
14.5	22.2	0.148	0.0116
13.0	18.1	0.197	0.0122
7.1	12.7	0.110	0.0226
6.6	12.7	0.082	0.0242
5.75	11.4	0.109	0.0252
19.6	34.2	0.123	0.0081

TABLE A - 2

SOLUBILITY AND DIFFUSIVITY DATA

A. Equilibrium Solubility of Gases in Water (26)

$x = P/K$, P in mm Hg, x is equilibrium mole fraction

Gas	Temperature (°C)	$K \times 10^{-7}$
Helium	20	9.50
	30	9.39
Oxygen	20	3.043
	21	3.100
	22	3.157
	23	3.215
	24	3.273
	25	3.330
	26	3.386
	27	3.444
	28	3.500
	29	3.555
	30	3.610
Carbon Dioxide	18	0.101
	19	0.104
	20	0.107
	21	0.111
	22	0.114
	23	0.117
	24	0.120
	25	0.124
	26	0.127
	27	0.130
	28	0.134
	29	0.137
	30	0.141
Propylene	14	0.384
	16	0.408
	18	0.432

TABLE A - 2 (Continued)

B. Propylene Solubility (2)

Temperature = 100°F

Pressure (psia)	x
10	0.47×10^{-4}
20	0.92×10^{-4}

C. Difusivity of Gases in Water (60) (Dilute Solutions)

Temperature = 25°C

Gas	$D \times 10^5$ (cm^2/sec)
Oxygen	2.41
Propylene	1.44
Carbon Dioxide	2.00
Helium	6.30

TABLE A - 3

OPERATING SPECIFICATIONS

Water Deaeration

Power (heating). . . . . 2250 Watt

Total Heating Time . . . . . 3 Hours (1 3/4 hrs. at boiling)

Water Circulation Rate . . . . . 0.3 GPM

Saturation and Purging of Gas

Purge Rate . . . . . 0.05 SCFM

Purge Time . . . . . 2 Hours

Mass Transfer Runs

Gas Volume (initial)

Oxygen, Helium. . . . . 2950 cc

Carbon Dioxide, Propylene . . . . . 4260 cc

Water Volume . . . . . 4600 cc

Water Level. . . . . .2 1/4 inches

Operating Pressure . . . . . .0.0 PSIG

TABLE A - 4

MASS TRANSFER DATA, OXYGEN - WATER

Note. Time in seconds, quantity absorbed in gm-moles x 10^5

Run # OX-O-41, O CPM

Time	Quantity Absorbed
100	0.0
700	4.1
1300	10.4
1900	16.6
3000	28.1
4600	45.1
6000	55.9
7500	68.3
9000	83.4

Run # OX-O-48, O CPM

Time	Quantity Absorbed
100	0.0
700	7.9
1500	20.3
2500	28.2
3500	43.9
4500	55.1
5400	63.0

Run # OX-3-47, 280 CPM

Time	Quantity Absorbed
100	0.0
700	7.9
1300	19.1
1900	32.3
2500	49.1
3100	65.6
3700	82.3
4400	101.1
5400	123.7

Run # OX-4-325, 400 CPM

Time	Quantity Absorbed
100	0.0
700	13.2
1300	27.7
1800	40.2
2400	55.1
3000	72.9
3600	90.0

TABLE A - 4 (Continued)

Run # OX-6-326, 600 CPM

Time	Quantity Absorbed
220	0.0
700	13.0
1300	28.8
1600	35.9
2100	51.0
2700	72.5
3300	97.7

Run # OX-6-46, 600 CPM

Time	Quantity Absorbed
100	0.0
700	12.7
1500	38.2
2500	70.7
3500	102.6
4500	133.9
5400	161.9

Run # OX-8-42, 800 CPM

Time	Quantity Absorbed
100	0.0
700	13.5
1300	30.0
1900	52.5
2500	69.9
3500	106.5
4500	134.5
5400	166.2

TABLE A - 5

MASS TRANSFER DATA, PROPYLENE-WATER

Note. Time in seconds, quantity absorbed in gm-moles x 10^4.

Run # PR-0-54, 0 CPM

Time	Quantity Absorbed
25	0.0
250	0.9
700	4.4
1700	10.7
2700	14.3
3700	16.6
4700	19.8
6000	22.8
7200	24.3

Run # PR-0-520, 0 CPM

Time	Quantity Absorbed
25	0.0
600	5.4
1700	10.6
2800	14.0
4000	16.4
5200	19.2
6600	20.6

Run # PR-4-519, 400 CPM

Time	Quantity Absorbed
25	0.0
500	6.4
1500	16.4
2500	24.8
3500	32.7
4500	40.0
5400	46.7

Run # PR-6-518, 600 CPM

Time	Quantity Absorbed
25	0.0
500	6.8
1500	19.6
2500	29.8
3500	38.6
4500	47.6
5400	55.2

Run # PR-8-516, 800 CPM

Time	Quantity Absorbed
25	0.0
600	8.9
1500	21.4
2500	36.7
3500	44.2

Run # PR-8-521, 800 CPM

Time	Quantity Absorbed
25	0.0
350	4.8
1400	18.2
2400	30.2
3400	40.5
4400	49.7
5400	58.2

TABLE A - 6

MASS TRANSFER DATA, HELIUM-WATER

Note. Time in seconds, quantity absorbed in gm-moles x 10^5

Run # HE-0-415, 0 CPM

Time	Quantity Absorbed
100	0.4
700	0.0
1500	7.3
2500	15.7
3500	23.1
4500	32.8
5400	39.5

Run # HE-0-49, 0 CPM

Time	Quantity Absorbed
100	4.5
700	0.0
1500	2.2
2500	8.9
3500	14.8
4500	23.3
5500	33.3
7000	42.8
8500	62.4

Run # HE-0-416, 0 CPM

(Air Saturated Water)

Time	Quantity Absorbed
100	0.0
500	- 3.5
1000	- 3.8
1500	- 4.0
2400	- 1.2
3500	3.8
4500	6.7
5400	10.1

Run # HE-4-410, 400 CPM

Time	Quantity Absorbed
100	0.0
700	2.6
1300	20.5
1900	27.7
3100	43.0
3700	72.1
4500	87.7
5400	109.7

TABLE A - 6 (Continued)

Run # HE-4-413, 400 CPM

Time	Quantity Absorbed
100	0.0
700	5.4
1500	21.0
2500	43.9
3500	62.9
4500	81.2
5400	97.8

Run # HE-6-411, 600 CPM

Time	Quantity Absorbed
100	0.0
700	11.9
1300	25.9
1900	39.1
2500	51.0
3100	65.6
3700	78.5
4500	94.1
5400	110.3

Run # HE-8-412, 800 CPM

Time	Quantity Absorbed
100	0.0
700	5.5
1300	25.0
1900	40.3
2500	54.6
3100	69.1

TABLE A - 7

MASS TRANSFER DATA, CARBON DIOXIDE - WATER

Note. Time in seconds, quantity absorbed in gm-moles x 10^3.

Run # C-0-425, 0 CPM

Time	Quantity Absorbed
25	0.0
200	2.2
500	5.4
900	9.5
1900	19.7
3000	29.8
4000	38.2
5000	46.1

Run # C-0-47, 0 CPM

(Delayed Water Inlet

Time	Quantity Absorbed
480	0.0
1300	9.0
2300	18.8
3425	28.7
4600	38.2

Run # C-0-429, 0 CPM

(Air Saturated Water)

Time	Quantity Absorbed
25	0.0
300	3.0
1000	9.6
2000	18.8
3000	27.4
4000	35.3
5000	42.9

Run # C-0-430, 0 CPM

Time	Quantity Absorbed
25	0.0
400	3.8
900	9.2
1900	19.1
3000	29.4
4000	38.1
5000	46.3
6000	54.3

Run # C-4-421, 400 CPM

Time	Quantity Absorbed
25	0.0
150	1.5
400	4.4
700	7.9
900	10.2
1500	16.2
1900	20.6
2400	24.9
3400	33.6
4400	41.9
5400	49.4

TABLE A - 7 (Continued)

Run # C-6-422, 600 CPM

Time	Quantity Absorbed
25	0.0
150	1.6
400	4.4
700	7.8
900	10.2
1400	15.4
1800	19.6
2800	28.9
3900	38.6
5100	48.3

Run # C-6-424, 600 CPM

Time	Quantity Absorbed
25	0.0
150	1.7
500	5.5
900	10.2
1700	18.6
2700	28.6
3700	37.4
4700	45.3

Run # C-8-423, 800 CPM

Time	Quantity Absorbed
25	0.0
150	1.7
350	4.2
800	9.9
1200	14.3
1700	20.2
2600	29.6
3500	38.0
4400	46.1
5400	54.4

Run # C-10.5-428, 1050 CPM

Time	Quantity Absorbed
25	0.0
200	2.6
700	9.6
1400	18.6
2250	28.2
3200	38.3
4200	47.5
5200	56.7

TABLE A - 8

EFFECTIVE DIFUSIVITY AND DIMENSIONLESS GROUPS

Gas	Frequency	$D_w \times 10^5$	D_w/D	Sc (Schmidt #)	$F\ (fh^2/D) \times 10^{-6}$
Oxygen	0	12.6	5.34	386	-
	0	11.5	5.05	412	-
	280	62.2	28.6	446	7.15
	400	71.4	32.1	432	9.88
	600	82.5	38.3	445	15.1
	800	90.5	39.7	412	19.15
Propylene	0	2.46	1.77	656	-
	0	2.52	1.57	505	-
	400	36.4	24.1	561	14.5
	600	41.0	26.6	535	21.2
	800	48.0	32.7	592	29.7
Helium	0	58.7	9.85	158	-
	0	54.5	10.0	186	-
	400	178	31.5	161	3.73
	600	214	38.8	181	5.92
	800	200	38.7	171	7.65
Carbon Dioxide	0	80.5	44.3	542	-
	0	76.5	43.0	555	-
	0	76.5	45.8	625	-
	400	76.5	43.1	562	12.4
	600	86.0	46.7	520	17.9
	600	93.0	47.2	460	16.7
	800	95.0	50.2	497	23.1
	1050	111	56.0	458	29.2

APPENDIX B

EXPERIMENTAL ERROR ESTIMATION FOR MASS TRANSFER EXPERIMENTS

The object of this estimation is to compute the error for the moles absorbed (Δ n) quantity in the mass transfer runs. The error is due to the experimental error in measuring pressure, volume and temperature.

By the ideal gas law, the quantity of gas at any time is

$$n = PV/RT \quad .$$

Using the typical values of 535°R as the temperature, 405.43 "water (1 atm.) as the pressure and the value 18.589(liter ("H_2O)/gm-mole °R) for R, get

$$n = 0.0407V \quad .$$

Typical values of V are 4.26 liters for Carbon Dioxide and Propylene and 2.95 liters for Oxygen and Helium. Therefore,

n = 0.119 gm-moles (O_2 and He)

n = 0.173 gm-moles (CO_2 and C_3H_6) .

The estimated experimental errors for the three properties are tabulated below.

Property	Estimated Error	Error Ratio
Temperature	$\pm$ 0.02 °R ($\pm$ 0.002 mv. on potentiometer)	$\delta T/T = \pm 0.02/535$
Pressure	$\pm$ 0.02 "water	$\delta P/P = \pm 0.02/405.43$
Volume (CO_2, C_3H_6)	$\pm$ 2cc	$\delta V/V = \pm 2/4260$
(O_2, He)	$\pm$ 0.02 cc	$\delta V/V = \pm 0.02/2950$

The effect of these errors on n is given by

$$\delta n/n = \delta T/T + \delta P/P + \delta V/V \quad .$$

Using the above values

$$\delta n/n = \pm 9.35 \times 10^{-5}, \quad \delta n = \pm 1.11 \times 10^{-6} \text{ gm-moles}$$

for Oxygen and Helium and

$$\delta n/n = \pm 55.6 \times 10^{-5}, \quad \delta n = \pm 9.65 \times 10^{-5} \text{ gm-moles}$$

for Carbon Dioxide and Propylene.

Since Δn is calculated from the difference of two values on n, the value of $\delta(\Delta n)$ is double that of δn. Thus, for any value of Δn in the data tabulation, the per cent error is given by

$$(\pm 2 (\delta n)/\Delta n) \times 100$$

where the values of δn are given above.

NOMENCLATURE

A	- Surface area, cm^2
A	- Constant in Equation (2-17)
a	- Wave Amplitude, cm
a	- Van der Waal constant, $atm(gm\text{-}mole)^2/liter^2$
a_v	- Van der Waal constant for gas
a_w	- Van der Waal constant for water
B	- Height of screen above wave surface, cm
B_c	- Height above surface of node ray intersection, cm
B_1, B_2	- Constants in Equation (2-12)
b	- Van der Waal constant, liter/gm-mole
b_v	- Van der Waal constant for gas
b_w	- Van der Waal constant for water
C	- Concentration, $gm\text{-}moles/cm^3$
C_i	- Equilibrium concentration, $gm\text{-}moles/cm^3$
C_b	- Bulk concentration, $gm\text{-}moles/cm^3$
C'	- Fluctuating component of concentration, $gm\text{-}moles/cm^3$
C^*	- Dimensionless concentration
C_p	- Specific heat, cal/gm-moles (°K)
c	- Wave velocity, cm/sec
D	- Molecular Diffusivity, cm^2/sec
D_w	- Effective Diffusivity, cm^2/sec
d	- Distance between node rays above wave surface, cm
d	- Change of volume during equipment measurement, cm^3
d	- Characteristic system dimension, cm

F - fh^2/D, dimensionless

f - Wave frequency, sec^{-1}

g - Acceleration due to gravity, cm^2/sec

Gr - Dimensionless Grashof Number

H_s - Heat of solution, cal/gm-mole

h - Depth of Liquid, cm

$\bar{J}$ - Total flux vector, gm-moles/cm^2(sec)

$\bar{J}_d$ - Surface flux of dilute component due to molecular diffusion

$\bar{J}_f$ - Surface flux of dilute component due to bulk flow

K - Constant in Equation (5-23)

K_1 - Empirical constant in Equation (5-39)

K_2 - Empirical constant in Equation (5-42)

k - Psuedo steady state mass transfer coefficient, cm/sec

L - B/λ, dimensionless

M - Molecular weight

m - a/λ, dimensionless

m - $2\pi/\lambda$, cm^{-1}

N - Surface flux of dilute component, gm-moles/cm^2(sec)

N - $1/\sigma\ (\partial\sigma/\partial z)$, dimensionless

Δn - Total gas absorbed, gm-moles

n - Refractive index

n - Index for summation in Equation (2-64)

$\bar{n}$ - Outward unit normal vector

P - Parachor

P - Pressure, atm

p - Pressure, atm

R - $D_w(2n+1)^2\pi^2\theta/4h^2$, dimensionless

R - Gas constant, liter atm/gm-mole(°K)

r - Exponential damping constant due to viscosity, cm^{-1}

S - d/λ, dimensionless

S - Control volume surface area, cm^2

Sc - Schmidt Number

T - Absolute temperature, °K

u - x direction velocity, cm/sec

V - Gas volume, cm^3

V - Control volume of liquid, cm^3

V_L - Liquid volume, cm^3

$\bar{v}$ - Bulk velocity, cm/sec

v - y direction velocity, cm/sec

v' - Fluctuating component of velocity, cm/sec

v^* - Dimensionless velocity

X - x direction displacement from mean position, cm

x - Horizontal Cartesian coordinate distance, cm

Y - y direction displacement from mean position, cm

y - Vertical Cartesian coordinate distance, cm (taken as positive upward)

y^* - Dimensionless distance

z - Mole fraction

α - Angle of tangent to wave surface with horizontal

α - Empirical exponent in Equation (5-39)

β - Constant in Equation (3-15), Reciprocal of 1/2 of generator travel, cm^{-1}

β - Empirical exponent in Equation (5-42)

Γ - $d\sigma/dC_i$, dyne (gm-mole)/cm^4

γ - Angle between emergent ray and vertical

γ - $(1/\rho)(d\rho/dz)$, dimensionless

δ - x direction light ray displacement, cm

δ - Film thickness, cm

ϵ - Eddy diffusivity, cm^2/sec

ϵ - Constant in Equation (3-15), cm^{-2}

η - Vertical displacement at free surface, cm

θ - Time, sec

θ_i - Angle of incidence

θ_r - Angle of refraction

λ - Wave length

μ - Viscosity, gm/cm sec

μ_s - Composite surface viscosity, gm/sec

ν - Kinematic viscosity, cm^2/sec

ρ - Density, gm/cm^3

ρ_L - Liquid density, gm/cm^3

ρ_m - Molar density, $gm\text{-}moles/cm^3$

ρ_v - Gas density, gm/cm^3

ρ_w - Density of water, gm/cm^3

σ - Surface tension, dyne/cm

σ_{yy} - y component of longitudinal surface stress, dyne/cm

σ^*_{yy} - Dimensionless Stress

ϕ - Velocity potential, sec^{-1}

ψ - Ratio of bouyant to wave potential energy

ψ_s - Ratio of surface tension to bouyant energy

ω - $2\pi f$, sec^{-1}

ω - Constant in Equation (5-16)

LITERATURE CITED

1. Addison, C. C.,Phil. Mag., 36, (7), 73 (1945)

2. Azarnoosh, A., The Solubility of Propane and That of Propylene in Water at Pressures to 500PSIA, M. S. Thesis, Univ. of Texas (1958)

3. Barnard, G. R., David Taylor Model Basin Instrument Division, Tech. Note #9, Sept. 1958

4. Bebner, A., J. Sci. Inst., 34, 506 (1957)

5. Bird, R. B., Advances in Chem. Engr., Vol.I, p.175, Academic Press (1956)

6. Bird, R. B., W. E. Stewart and E. N. Lightfoot, Transport Phenomena, p.645, John Wiley and Sons (1960)

7. Ibid., p.580

8. Bond, J. and M. D. Donald, Chem. Eng. Sci., 6, 237 (1957)

9. Brock, J. R. and R. B. Bird, AIChE Journal, 1, 174 (1955)

10. Carry, C., La Houille Blanche, 11, 75 (1956)

11. Carslaw, H. S. and J. C. Jaeger, Conduction of Heat in Solids (2nd ed.), p.100, Oxford Press (1959)

12. Chapman, J. A., The Effect of Small Surface Waves on Mass Transfer Rate, M.S. Thesis, Oklahoma State University (1961)

13. Chiang, S. H. and H. L. Toor, AIChE Journal, 5, 165 (1959)

14. Chien, N., Am. Geophysical Union Trans, 35, 897 (1954)

15. Clark, C. B., Amer. J. Physics, 27, 478 (1959)

16. Coulson, C. A., Waves (7th ed.), p.60-84, Interscience Publishers (1955)

17. Crapper, G. D., J. Fluid Mech., 2, 532 (1957)

18. Cullen, E. J. and J. E. Davidson, Chem. Eng. Sci., 6, 49 (1956)

19. Danckwerts, P. V., Ind. Eng. Chem., 43, 1460 (1951)

20. Faller, A. J., Am. Geophysical Union Trans., 39, 716 (1958)

21. Ferguson, A., Phil. Mag., 28, 403 (1914)

22. Glasstone, S., Elements of Physical Chemistry, p.157, Van Nostrand (1946)

23. Grimley, S. S., Trans. Inst. Chem. Engrs. (London), 23, 228 (1945)

24. Hanratty, T. J. and J. M. Engen, AIChE Journal, 3, 299 (1957)

25. Hanratty, T. J. and A. Hershman, AIChE Journal, 7, 488 (1961)

26. International Critical Tables, Vol. III, p.254, McGraw Hill (1928)

27. Jackson, M. L., AIChE Journal, 1, 231 (1955)

28. King, J. L., P. Boyle and J. B. Ogle, J. Fluid Mech., 4, 283 (1958)

29. Kuper, C. G. and D. H. Trevena, Phys. Soc. Proc., 65, 46 (1952)

30. Lemlich, R. and M. R. Levy, AIChE Journal, 7, 240 (1961)

31. Levich, V. G., Physiocochemical Hydrodynamics, p.683-9, Prentice Hall (1962)

32. Ibid., p.127

33. Lilleleht, L. U. and T. J. Hanratty, AIChE Journal, 7, 548 (1961)

34. Lilleleht, L. U. and T. J. Hanratty, J. Fluid Mech., 11, 65 (1961)

35. Longuet-Higgins, M. S., Roy. Soc. London Phil. Trans., 245, 535 (1953)

36. Longuet-Higgins, M. S., J. Fluid Mech., 8, 293 (1960)

37. McAdams, W. H., Heat Transmission (3rd ed.), p.180, McGraw Hill (1954)

38. Meszaros, L., Acta Unv. Szegediensis, Acta Phys. et Chem., 4, 165 (1958), (in English)

39. Muenz, K. and J. M. Marchello, Rev. Sci. Inst., 35, 953 (1964)

40. Othmer, D. F. and R. Gilmont, Petrol, Refiner, 31, 107 (1952)

41. Page, L., Introduction to Theoretical Physics (3rd ed.), p.265, Van Nostrand (1952)

42. Perry, R. H., C. H. Chilton and S. D. Kirkpatrick, Chemical Engineers Handbook (4th ed.), p.3-70, McGraw Hill (1963)

43. Ibid., p.5-57

44. Railly, J. W. and B. F. Scott, J. Sci. Inst., 38, 442 (1961)

45. Raimondi, P. and H. L. Toor, AIChE Journal, 5, 86 (1959)

46. Ruellan, F. and A. Wallet, La Houille Blanche, 5, 483 (1950)

47. Schlichting, H., Boundary Layer Theory, p.461, McGraw Hill (1950)

48. Schooley, A. H., Proc. Nat. Electronics Conf., 5, 303 (1949)

49. Scriven, L. E., Chem. Eng. Sci., 12, 98 (1960)

50. Scriven, L. E. and R. L. Pigford, AIChE Journal, 4, 439 (1958)

51. Shenck, H. Jr., J. Optical Soc. Amer., 47, 653 (1957)

52. Sternling, C. B. and L. E. Scriven, AIChE Journal, 5, 514 (1959)

53. Stoker, J. J., Water Waves, Interscience Publishers (1957)

54. Stong, C. L., Sci. Amer., 144 (October 1962)

55. Striba, C. and O. H. Hurt, AIChE Journal, 1, 178 (1955)

56. Tadjebakhsh, I. and J. B. Keller, J. Fluid Mech., 8, 442 (1960)

57. Tailby, S. P. and S. Portalski, Chem. Eng. Sci., 17, 283 (1962)

58. Tucker, M. J. and H. Charnock, Proc. Fifth Conf. on Coastal Eng., Chap. 14 (1954)

59. Ursell, F., R. G. Dean and Y. S. Yu, J. Fluid Mech., 8, 33 (1960)

60. Vivian, J. E. and C. J. King, AIChE Journal, 10, 520 (1964)

61. Wehausen, J. V. and E. V. Laitone, Encyclopedia of Physics, Vol. IX, Springer Verlag (1960)

62. Ibid., p.461-9

63. Ibid., p.638-46

64. Whitham, G. B., J. Fluid Mech., 12, 135 (1962)

65. Whittenbury, C. G., E. A. Huber and G. S. Newell, Rev. Sci. Inst., 30, 674 (1959)

66. Wilke, C. R., J. M. Prausnitz and A. Acrivos, Ind. Eng. Chem., 51, 466 (1959)

67. Wilner, L. B., Rev. Sci. Inst., 31, 501 (1960)

68. Yu, Y. S. and F. Ursell, J. Fluid Mech., 11, 529 (1961)